Research article

Eocene to Oligocene high paleolatitude neritic record of Oi-1 glaciation in the Otway Basin southeast Australia

Stephen J. Gallagher[a,*], Bridget Wade[b], Li Qianyu[c], Guy R. Holdgate[a], Paul Bown[b], Vera A. Korasidis[a,h], Howie Scher[d], Alexander J.P. Houben[e,1], Brian McGowran[f], Tony Allan[g]

[a] School of Earth Sciences, University of Melbourne, Melbourne, Victoria 3010, Australia,
[b] Department of Earth Sciences, University College London, Gower Street, London WC1E 6BT, United Kingdom.
[c] School of Ocean and Earth Sciences, Tongji University, Shanghai 200092, China
[d] School of the Earth, Ocean and Environment, University of South Carolina, 701 Sumter Street, EWS 617, Columbia, SC 29208, USA
[e] Marine Palynology and Paleoceanography, Laboratory of Palaeobotany and Palynology, Department of Earth Sciences, Faculty of Geosciences, Utrecht University, Utrecht, the Netherlands
[f] School of Earth & Environmental Sciences, Mawson DX 650 313, The University of Adelaide, Adelaide, SA 5005, Australia
[g] CSIRO (Energy), 11 Julius Avenue, North Ryde, New South Wales 2113, Australia
[h] Department of Paleobiology, National Museum of Natural History, Smithsonian Institution, Washington, DC 20013, USA

A B S T R A C T

Multiple stable isotope investigations from upper Eocene to lower Oligocene deep-water marine sequences record the transition from global greenhouse to the icehouse conditions (Oi-1 glacial). While Southern Ocean high latitude deep sea records of this transition are well known, their shallow marine equivalents are rare and have the potential to record the eustatic and oceanic consequences of Paleogene glacial variability. The well-known high paleolatitude (~55°S) neritic carbonate sequence at Browns Creek and Castle Cove in the Otway Basin in southeast Australia spans the Eocene-Oligocene boundary. During this time the area lay on the northeastern margin of the Australo-Antarctic Gulf facing the evolving Southern Ocean. The importance of this record has been hampered by a lack of a consistent stratigraphy and contradictory microfossil interpretations. To reconcile these issues we combine new bio-, chemo- and lithostratigraphic analyses of the outcrops and a new core (Colac-2) with pre-existing data to revise the stratigraphy. This confirms the middle/upper Eocene boundary is near the base of the section. The overlying upper Eocene siliciclastic strata are truncated by an unconformity (of ~0.8 Ma in duration) and overlain by glauconitic sand (the *Notrostrea* greensand) deposited after ~35.9 Ma. Subsequently deepening to middle to outer neritic depths deposited cyclic carbonates. Shallowing after ~35 Ma deposited laterally variable calcareous siliciclastic facies. These strata were tilted and eroded prior to 34 Ma leading to shallow water facies that may have been subaerially exposed during uplift. Brachiopod strontium isotope dates and an 0.5‰ carbon isotope excursion above this unconformity suggests the top of the Browns Creek and the base of the Castle Cove section correlate to Eocene-Oligocene transition (EOT-1) at ~34 Ma. The subsequent persistence of positive C/O isotope values above this level records the transition to the Oi-1 glaciation at ~33.7 Ma. Strong cyclicity in the inner shelf Castle Cove limestone is interpreted to record the commencement of obliquity dominated glacio-eustacy during the Oi-1 glacial phase. The shallowing from outer to inner shelf palaeodepths from the late Eocene to the early Oligocene is likely related to the onset of cryosphere expansion, however, palaeodepth estimates are complicated by the onset of regional compressional tectonism at the Eocene/Oligocene boundary that caused localized tilting and an unconformity with possible antisiphoning effects in this near-field site.

1. Introduction

There has been a long-term change to a cooler, ice sheet-prone planet since the Cretaceous period. One of the largest climate shifts was around the Eocene/Oligocene boundary (E/O). Prior to the E/O, deep ocean oxygen isotope records suggest that the Antarctic icesheet was

---

small and transient (*"the icehouse cometh"*, Browning et al., 1996), however by the Oligocene the icesheet was expansive, reaching the Antarctic coast line (Zachos et al., 1996, 2001, 2008). A driver implicated in this change was the opening of the Southern Ocean and the onset of the Antarctic Circumpolar Current (ACC) during the early Oligocene thermally isolating Antarctica (Kennett, 1977). However, the timing of onset of the ACC is estimated as either too early at ~40 Ma (Scher and Martin, 2006), or too late at ~30 Ma (Katz et al., 2011; Hill et al., 2013; Scher et al., 2015) to be the ultimate trigger. A more likely cause of cryosphere expansion is declining atmospheric CO_2 from high CO_2 greenhouse conditions of the early Cenozoic Earth (Pearson et al., 2009), which culminated in East Antarctic Ice Sheet expansion by the early Oligocene and the onset of icehouse conditions (Zachos et al., 2001, 2008; Oi-1– 33.7 Ma). CO_2 estimates in the late Eocene decline from > 1200 to ~900 ppmv just prior to the Eocene/Oligocene boundary before falling to > 700 ppmv during Oi (Pearson et al., 2009; Zheng et al., 2013) suggesting CO_2 decline was the primary driver of glacial expansion on Antarctica (Pearson et al., 2009; Pagani et al., 2011).

High southern paleolatitude outcrop records of the EOT are sparse, where, subsurface records are primarily derived from deep water IODP (International Ocean Discovery Program and its predecessors: e.g. Houben et al., 2013), other coring expeditions around Antarctica (e.g. Galeotti et al., 2016) and limited onshore and offshore cores from southeast Australia (Gallagher et al., 2013; Korasidis et al., 2019). Southeast Australia lay just north of 60°S during the late Eocene (Fig. 1). In this paper we describe a neritic carbonate outcrop (Browns Creek and Castle Cove) and subsurface (Colac-2 core) record across the Eocene/Oligocene boundary in the Otway Basin (Fig. 1). The outcrop sections have had a long history of (bio)stratigraphic analyses (see summaries in Kamp et al., 1990; Shafik and Idnurm, 1997; Holdgate and Gallagher, 2003; McGowran, 2009; Houben et al., 2019a), suggesting that it is one of the best exposed neritic sequences spanning the Eocene-Oligocene transition on the northern margin of the Australo-Antarctic Gulf. The section has the potential to reveal eustatic evidence for Paleogene glacial events. However, as the sections are exposed in several discontinuous outcrops previous studies have not been able to satisfactorily erect a consistent stratigraphy to form a framework for biostratigraphic analyses. In addition to the stratigraphic problems there are biostratigraphic discrepancies in the section that need clarification before this section can be directly compared to deeper oceanic archives. The aims of this paper are to: 1. describe the lithostratigraphy of these neritic carbonate outcrops and an adjacent core (Colac-2) using new facies analyses, outcrop and subsurface gamma logging and carbonate analyses; 2. biochronologically calibrate the sections using new and pre-existing foraminiferal, palynological (spores/pollen/dinocysts) and nannofossil analyses; 3. use new brachiopod (Sr) isotope dates with $\delta^{18}O/\delta^{13}C$ benthic foraminiferal data together with pre-existing magnetostratigraphic data to constrain the chronology; and 4. to correlate these strata with deeper water high paleolatitude Ocean Drilling Program (ODP) Sites; and to identify the E/O boundary and Oi events.

2. Geological setting

The Otway Basin (Fig. 1) is one of a series of basins along Australia's southern margin that formed after the breakup of Australia from Antarctica. It consists of Cretaceous to recent strata that initially were deposited in rift related terrestrial environments and transitioned to a sag phase with fully marine conditions by the Paleogene (Gallagher and Holdgate, 2000; Gallagher et al., 1999; Holdgate and Gallagher, 2003; Frieling et al., 2018). Cenozoic strata in this basin are up to 2.5 km thick in the offshore region and are extensive yet thinner in the subsurface onshore area. Outcrops are common along the Otway coast where Neogene neotectonics (Dickinson et al., 2001; Dickinson et al., 2002) have tilted and exposed a series of Paleogene to Neogene strata near the Otway ranges (Fig. 1). The strata investigated in this paper

include the outcrops at Browns Creek (West and East gullies, Figs. 1 to 4) and Castle Cove (Figs. 1, 5) with a subsurface section in Colac-2 (Figs. 1, 6; drilled by Geoscience Australia in 2003; 38.7594°S; 143.38235°E). Paleogene marine siliciclastic strata of the Johanna River sands (Carter, 1958) of the Mepunga Formation (Gallagher and Holdgate, 2000; Holdgate and Gallagher, 2003) unconformably overlie the Cretaceous Otway Group in this area (Fig. 1). These are in turn overlain by the Browns Creek clays and Castle Cove limestone (Carter, 1958) of the Eocene to Oligocene Narrawaturk Formation (Gallagher and Holdgate, 2000; Holdgate and Gallagher, 2003). Undifferentiated terrestrial Cenozoic to Quaternary siliciclastic strata overlie these units (Fig. 1).

Additional informal units have previously been recognized in the Browns Creek clays in two gulleys here denoted Browns Creek East (BCE) and Browns Creek West (BCW) (Fig. 1; Raggatt and Crespin, 1955; Cookson and Eisenack, 1965; McGowran, 1978; Tickell et al., 1992; Abele, 1994; McGowran, 2009):

1. Browns Creek East: the lower unit with 8 to 9 m of *Turritella*-rich dark grey to black clay overlain by a 2 m-thick shelly glauconitic greensand, with a horizon of *Notostrea* (the *Notostrea* Greensand, Fig. 3). 18 m of "banded" grey bryozoal clayey marl over lie this greensand.
2. The section continues in Browns Creek West (Fig. 4) with over 10 m of dark grey carbonaceous marl, *Turritella* clay, and marl (Tickell et al., 1992; Abele, 1994) in section that partially overlaps with BCE, however, the correlations between the gullies in these papers are not well constrained.

The Browns Creek clays also outcrop in Castle Cove (CC, Fig. 5), although their relationship to BCE and BCW have not previously been determined, however, they are interpreted to stratigraphically overlie the uppermost interval of BCE (McGowran, 1978; Waghorn, 1989; Kamp et al., 1990; Tickell et al., 1992). In CC the Browns Creek clays consist of 3 m of glauconitic marl that are overlain by ~16 m of "fawn" clay alternating with thin limestone bands (Carter, 1958). Over 20 m of Castle Cove limestone overlies the Browns Creek clays in this section (Fig. 5). This limestone unit is distinguished by its alternating interbeds of "gritty" limestones with brown sandy clay and marls (Carter, 1958).

The section has a long history of micropaleontological investigation and we include a brief synopsis here, as we will incorporate some of these data in this paper to determine the detailed stratigraphy and correlations between the outcrop and subcrop sections. Parr (1947) documented the genus *Hantkenina alabamensis* in the *Notostrea* greensand and interpreted an Eocene age for the section. More detailed work was carried out by Carter (1958) who first described the informal units Johanna River sands, Browns Creek clays and Castle Cove limestone. Carter also outlined benthic and planktic foraminiferal faunas in these units assigning them an Eocene age based on the presence of *Globigerinatheka index* and *Subbotina linaperta*. Cookson and Eisenack (1965) described several new species of microplankton from BCE. McGowran (1978, 2009) listed key planktic foraminiferal species in the section noting the top of *Acarinina collactea* and rare *A. primitiva* near the base of the Browns Creek clays indicating the middle/upper Eocene boundary. McGowran (1978) also noted the Top *G. index* and *Tenuitella insolita* in the Castle Cove limestone with the Top common *G. index* in the uppermost metre of BCW (McGowran, 2009). Shafik (1981, 1983, 1989, 1995) and Shafik and Idnurm (1997) described nannofossil assemblage datums and their relationship to foraminiferal datums and magnetostratigraphy in the lower 10 m of BCE to the top of the *Notostrea* greensand. This work confirmed the middle to late Eocene age for this part of the section. Waghorn (1989) and Kamp et al. (1990) used additional nannofossil (top *Discoaster saipanensis*) and planktic foraminiferal isotope data (a $\delta^{18}O$ excursion) from BCE and CC to suggest that the Eocene/Oligocene boundary was in the Browns Creek clays above 17 m log level in BCE (Fig. 3) and at the base of the CC
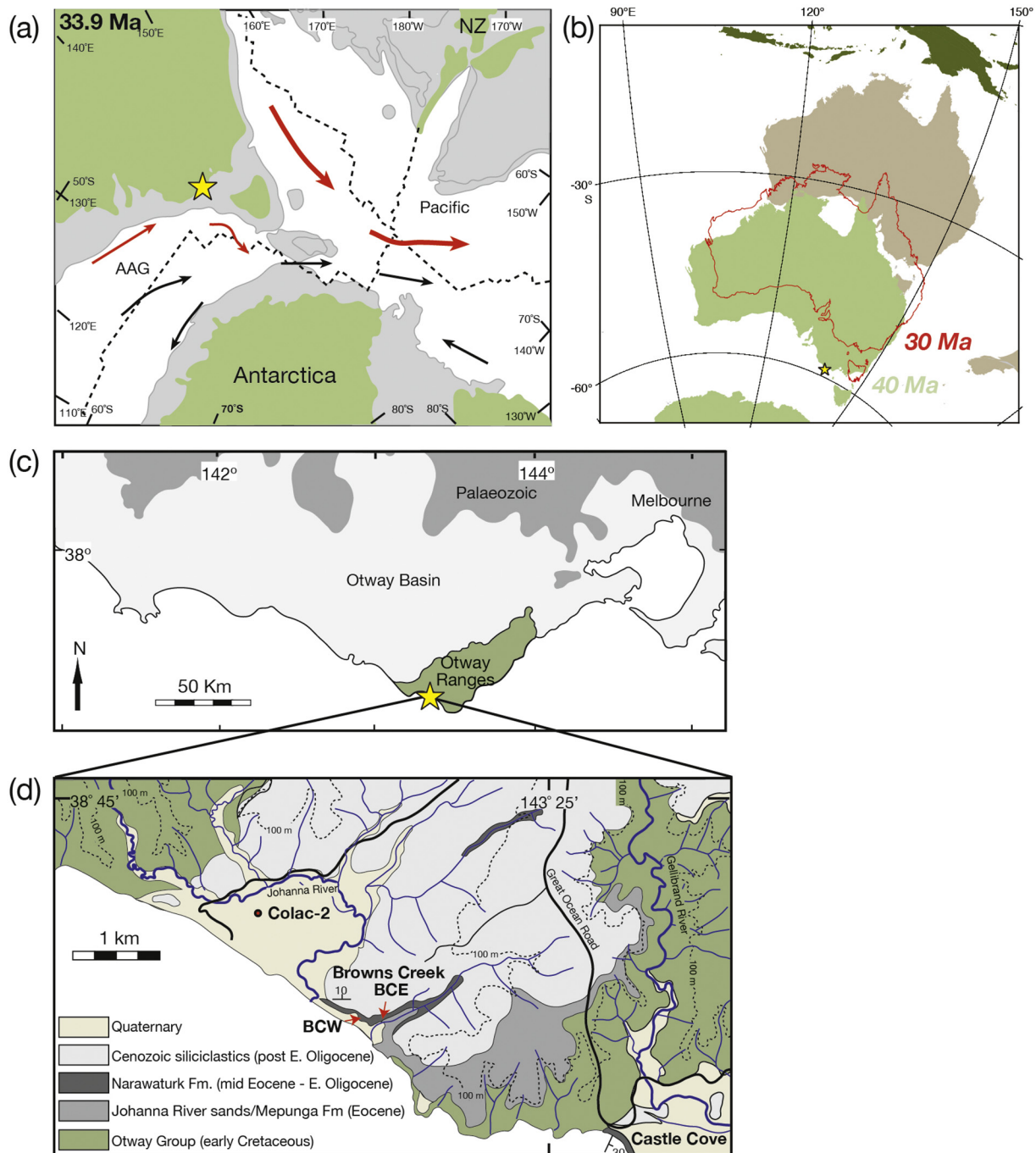
Fig. 1. Location of the sections. (a) Paleogeographic reconstruction of southeast Australia at the Eocene-Oligocene boundary, red arrows are warm currents, black arrows are cool currents (adapted from Stickley et al., 2004), AAG = Australo-Antarctic Gulf. (b) Plate tectonic motions of Australia from 40 (green) to 30 Ma (red outline) to today (brown) adapted from Gallagher et al. (2017). (c) and (d) Regional geology of Browns Creek and Castle Cove and Colac-2 core (adapted from Tickell et al., 1992). BCW = Browns Creek West and BCE = Browns Creek East. The location of the Otway section is the yellow star in (a), (b) and (c). (For interpretation of the references to colour in this figure legend, the reader is referred to the web version of this article.)

section (Fig. 5) ~35 m below the top of *G. index* reported by McGowran (1978) and Abele (1994). The foraminiferal and nannofossil data of the literature above were reviewed and additional foraminiferal data obtained by Abele (1994) for BCE, BCW and CC. This suggests that the middle/upper Eocene boundary is near the base of BCE and that the Top *T. insolita* is in the upper part of the Browns Creek clays and Top *G. index* near the top of the Castle Cove limestone, just below an interpreted Eocene/Oligocene boundary at Castle Cove. Waghorn (1989) and Kamp et al. (1990) interpreted their nannofossil datum to be isochronous with global datums and used them to locate the Eocene/

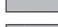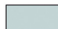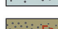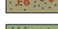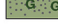Oligocene boundary and suggested typically Eocene foraminiferal taxa (*Globigerinatheka index*) survived past this boundary. However, Abele (1994) suggested that these nannofossil datums were diachronous and the foraminiferal datums isochronous. The various interpretations in the review above demonstrates that the location of the Eocene/Oligocene boundary in these outcrops is not clear. In this work we combine previous data (and have reanalysed all of Abele's (2004) samples) with new biostratigraphic and chronostratigraphic data to interpret the stratigraphy of this high paleolatitude neritic section.

Table 1
Replicate analyses of six batches of brachiopods from BCE. The standard error (s.e.) uncertainty is calculated using Student's *t*-test as outlined in McArthur et al. (2001).

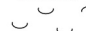| Sample ID	BCE log ht. m	87Sr/86Sr	2 s error
B8a	8	0.707739	0.000010
B8b	8	0.707745	0.000010
Mean		0.707742	0.000010
Value of Student's t		6.2050	
s.e. at 95% confidence interval		0.0000395	
n		2	
Ratio normalized to NBS987 = 0.710248		0.707755	
B8.5a	8.5	0.707748	0.000010
B8.5b	8.5	0.707735	0.000009
Mean		0.707742	0.000010
Value of Student's t		6.2050	
s.e. at 95% confidence interval		0.0000395	
n		2	
Ratio normalized to NBS987 = 0.710248		0.707755	
B9.5a	9.5	0.707748	0.000008
B9.5c	9.5	0.707741	0.000008
B9.5d	9.5	0.707739	0.000011
B9.5e	9.5	0.707741	0.000008
Mean		0.707742	0.000009
Value of Student's t		3.4940	
s.e. at 95% confidence interval		0.0000157	
n		4	
Ratio normalized to NBS987 = 0.710248		0.707755	
B18a	18	0.707771	0.000013
B18b	18	0.707746	0.000009
Mean		0.707759	0.000011
Value of Student's t		6.2050	
s.e. at 95% confidence interval		0.0000395	
n		2	
Ratio normalized to NBS987 = 0.710248		0.707772	
B25a	25	0.707795	0.000010
B25b	25	0.707795	0.000008
Mean		0.707795	0.000009
Value of Student's t		6.2050	
s.e. at 95% confidence interval		0.000039	
n		2	
Ratio normalized to NBS987 = 0.710248		0.707808	
B26a	26	0.707792	0.000010
B26c	26	0.707796	0.000008
B26e	26	0.707797	0.000009
B26b	26	0.707806	0.000010
B26d	26	0.707783	0.000009
B26f	26	0.707791	0.000007
Mean		0.707794	0.000009
Value of Student's t		2.9690	
s.e. at 95% confidence interval		0.000011	
n		6	
Ratio normalized to NBS987 = 0.710248		0.707807	

Lithology

Calcareous clay

Clayey marl - wackestone

Marl - wackestone

Sandy marl - wackestone

Calcisiltite - packstone

Limestone - packstone/grainstone

Sandy limestone - packstone/grainstone

Ferruginous calcareous sand

Glauconitic calcareous sand

Ferruginized horizon

G G Glauconite

Fossils

Bivalve

Brachiopod

Turritella

Notostrea

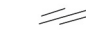**Physical structures**

Lamination

Cross bedding

Burrow horizon

Nodular horizon

Fig. 2. Key to logs in Figs. 3 to 13.

3. Methods

3.1. Facies analyses and stratigraphic logging

Outcrop facies were logged, sampled and measured using a Jacobs staff (Fig. 3-5). Colac-2 core was logged (Fig. 6). While logging, the natural gamma content of each outcrop section was measured using a portable handheld radiation detector (RS-230 BGO Super-SPEC) at ~25 to ~50 cm intervals. This yielded values for total gamma (ppm, parts per million), K (%), U (ppm) and Th (ppm). An industry standard down hole (total) gamma log was acquired for Colac-2 measured in API units. %Carbonate content analyses using the volumetric technique of Wallace et al. (2002) were carried out on two hundred and sixty-four samples (Fig. 7). The facies are based on field observations and further classified using carbonate content and grain size using the limestone/marl/clay classification by Pettijohn (1975) and the textural classification of Dunham (1962). The facies, %carbonate and multispectral gamma data were used to correlate the strata from the subsurface (Colac-2) and between the outcrops (Fig. 7).

3.2. Foraminiferal analyses

209 samples were processed from all sections for foraminifera by standard microfossil techniques and split using a microsplitter for counting. Residues from BCE, BCW and CC were picked for foraminiferal *Cibicidoides* spp. stable isotope analyses (see below, Fig. 8). Around 250 planktic and benthic foraminifera were counted in the ≥63 μm fraction of the 79 samples in Colac-2 (Fig. 9). Over 600 foraminifera were counted in the ≥63 μm fraction of each of the 29 samples from BCW, 70 from BCE and 28 samples from CC (Figs. 9, 10). The percentage planktics in the total foraminiferal assemblage was calculated (Fig. 9). Quantitative and semi-quantitative biostratigraphically significant planktic taxa are plotted (Fig. 10, Supplementary Table S1). This figure includes data from all the outcrop microfossil samples analysed by Abele (1994). We have rechecked the planktic foraminiferal identification in all Abele's samples and have found these data are robust (discussed below). The foraminiferal taxonomy follows that of Gallagher et al. (1999), Gallagher and Holdgate (2000), Pearson et al. (2006) and Wade et al. (2018).

3.3. Nannofossil analyses

22 samples (Fig. 11, Supplementary Table S1) were prepared as smear slides (Bown and Young, 1998) and analysed using a Zeiss Axiophot microscope at x 1000 magnification in cross polarised and phase contrast light. Assemblages were logged semi-quantitatively. The nannofossil biozones of Martini (1971) were used, with additional events considered from Okada and Bukry (1980) calibrated to the Gradstein et al. (2012) timescale. Key biostratigraphically important taxa are plotted (Fig. 9) combined with data from Shafik (1981, 1983, 1989, 1995); Shafik and Idnurm (1997); Waghorn, (1989) and Kamp et al. (1990).

3.4. Palynological analyses

15 samples from BCE and BCW were processed for palynological analyses following standardized methods used at the Laboratory of Palaeobotany and Palynology, Utrecht University, The Netherlands (Houben et al., 2019a). In brief, freeze-dried samples were processed for semi-quantitative analyses (including the addition of *Lycopodium* marker spores) using 30% hydrochloric acid and 38% hydrofluoric acid. Residues were placed in an ultrasonic bath for a maximum of 5 min and sieved over a 15 μm mesh. Slides were analysed at 500 X magnification to a minimum of 200 dinocysts. When dinocyst counts were low, counting was stopped after 2 slides. When less than 50 dinocysts were identified after the counting of 2 slides, results were
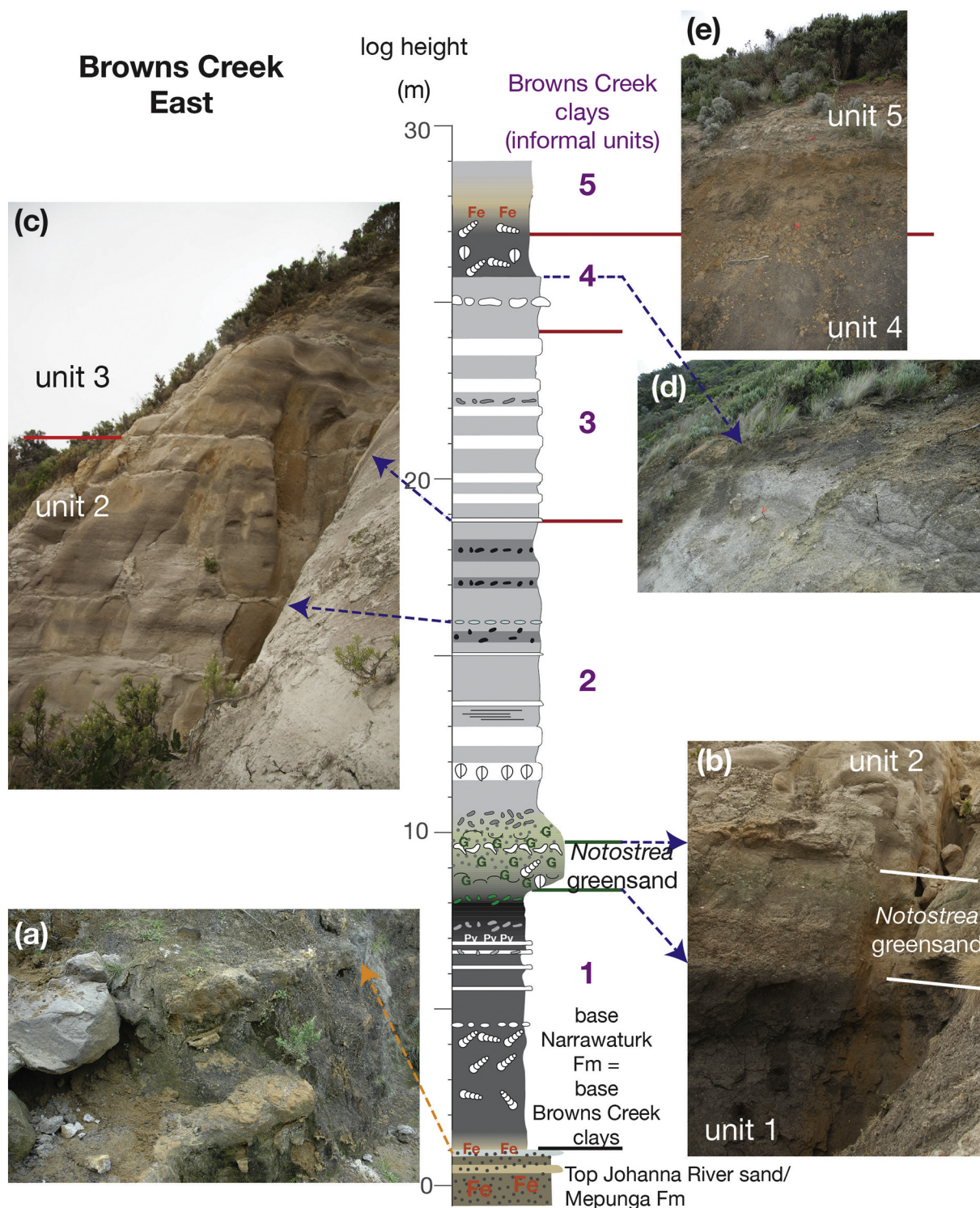
Fig. 3. Browns Creek East. Informal units in the Browns Creek clays are numbered 1 to 5 with the exception of the *Notostrea* greensand which is a unit between units 1 and 2. (a) Two calcareous beds in the sandy ferruginous Johanna River sand/Mepunga Formation. (b) *Notostrea* greensand (~2 m thick) overlying the calcareous clay of unit 1. (c) Metre scale cyclic alternations of clayey marls, marls (wackestones) and calcisiltites (packstones) in the Browns Creek clays looking west, the vertical thickness between the lower nodule bed and the unit 2/3 boundary is 3 m. (d) Boundary between the grey marl (wackestone) and the "upper dark" calcareous clay in unit 4. (e) 2.5 m of the uppermost section showing the transition from the calcareous clay of unit 4 to ferruginized marl of unit 5.

discarded for qualitative analysis. Dinocyst nomenclature and taxonomy, unless stated otherwise, are based on the work of Fensome et al. (2008). Taxonomy of spinose Transantarctic dinocyst taxa (*Vozzhenni-kovia, Spinidinium*) follows Sluijs et al. (2009). A further 48 samples were processed for palynofloras by Global Geolab in Canada using standard palynological processing techniques including HCl and HF acid digestion, heavy liquid separation and oxidation with nitric acid. These samples were analysed for spore-pollen biostratigraphy using the palynological zonation schemes of Stover and Partridge (1973) and Partridge (1999). Slides were analysed on a Zeiss AxioScope A1 microscope.
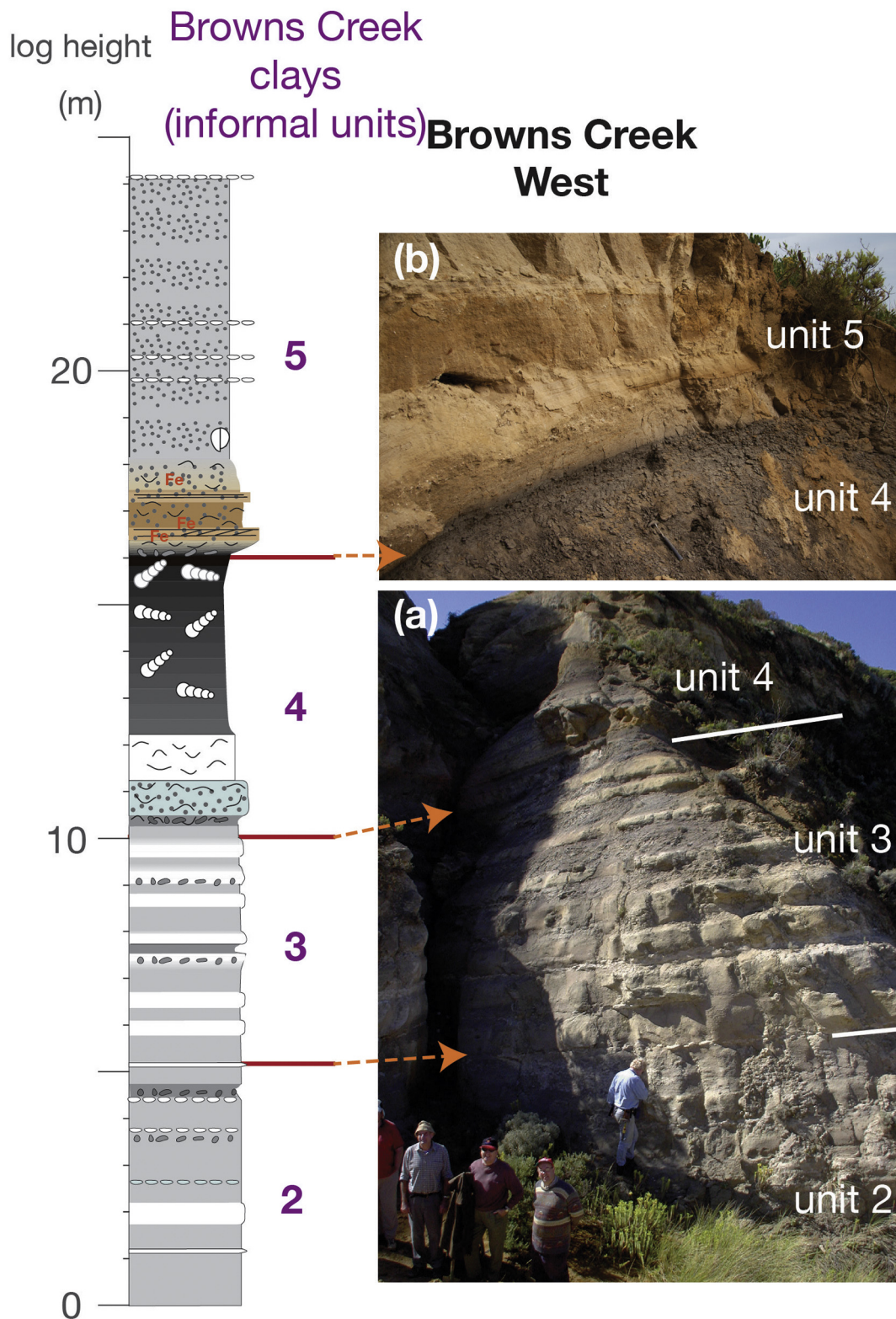
Fig. 4. Browns Creek West. Browns Creek clays informal units described are numbered 2 to 5. (a) Metre scale cyclic alternations of marls (wackestones) and calcisiltites (packstones) in units 2 to 4 of the Browns Creek clays, the vertical thickness of unit 3 is ~5 m. (b) Boundary between the calcareous clay (unit 4) and basal ferruginous calcareous sand of unit 5.

3.5. Benthic foraminiferal oxygen/carbon isotope analyses

Out of the 127 outcrop samples analysed for foraminifera, only 50 samples yielded sufficient quantities (two to three specimens > 150 μm) of well-preserved *Cibicidoides* spp. (Fig. 8; Supplementary Table S1). Stable isotope analyses were performed at the University College of London (UCL) Bloomsbury Environmental Isotope Facility using a Gas Bench II device. Analytical precision was within 0.04 and 0.08‰ for $\delta^{13}C$ and $\delta^{18}O$, respectively. All unknowns were analysed with international and internal standards of similar
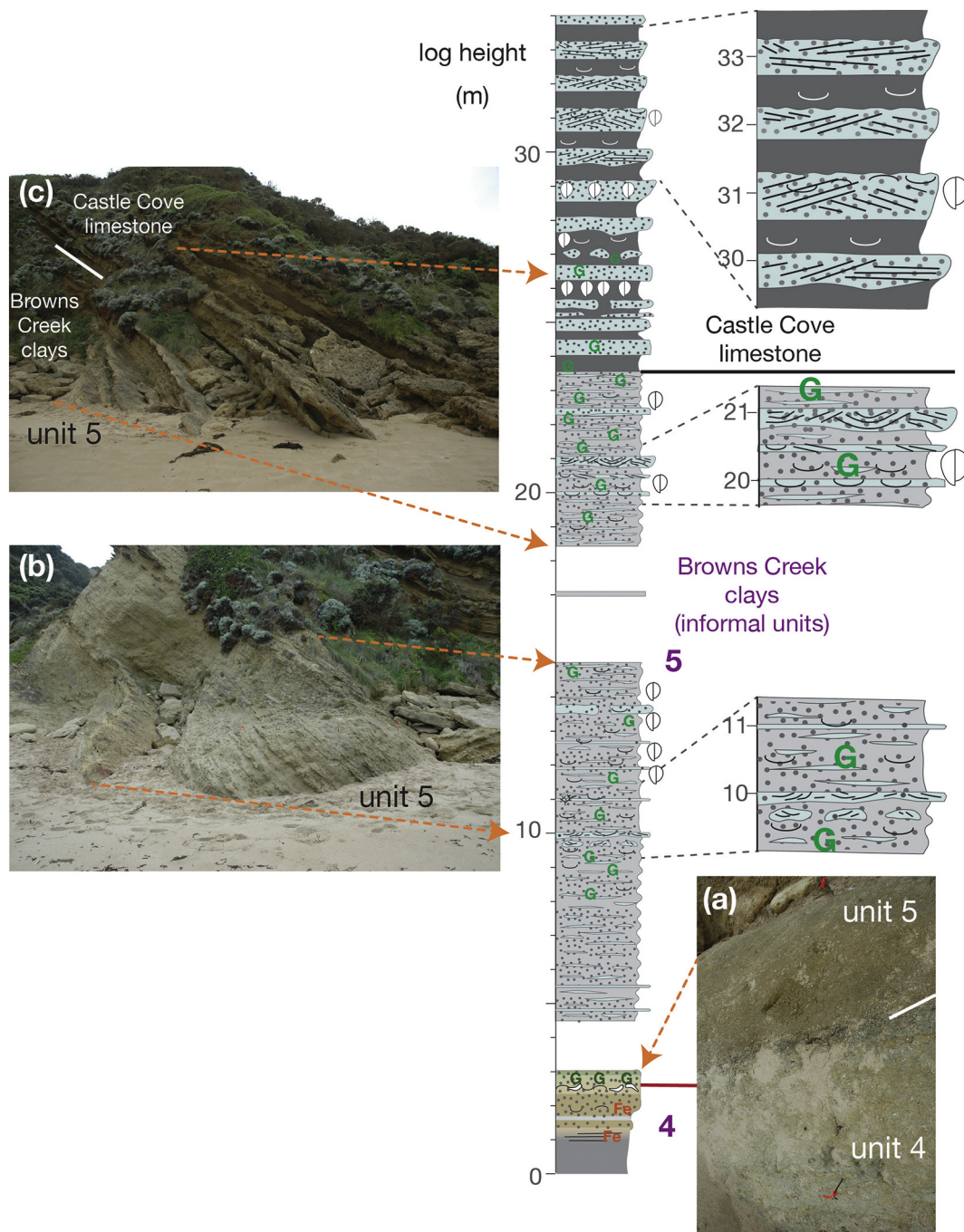
Fig. 5. Castle Cove, log height in metres. Browns Creek clays informal units are numbered 4 to 5. (a) Basal 2 m of CC with the boundary between unit 4 and 5 denoted by a glauconitic calcareous sand (~1 m thick). (c) Boundary between the sandy marl/limestones of unit 5 and the Castle Cove limestone with its distinctive meter scale alternations of sandy limestones (packstone/grainstones) and calcareous clays (thickness between the orange arrows is ~8 m). (b) Well-bedded sandy limestones (packstone/grainstones) and sandy marls (wackestones) of unit 5, the outcrop of unit 5 here is ~10 m thick.

weight. Isotopic ratios are reported as δ values relative to the Vienna Pee Dee Belemnite standard (VPDB).

3.6. Strontium isotope analyses

18 terebratulid brachiopods were collected from six horizons in BCE (Fig. 12). Eight brachiopods were collected from eight horizons in CC (Fig. 12). All samples were prepared according to the method outlined in McLaren et al. (2009). They were cleaned and washed using dilute hydrochloric acid. Each brachiopod was powdered using an agate mortar and pestle. Powders were dissolved in 1 M acetic acid to

minimise extraction of Sr from clays and other terrigenous material (e.g. DePaolo and Ingram, 1985), and strontium extraction followed standard methods of ion exchange.

The BCE brachiopod isotopic compositions were measured on a VG 354 thermal ionisation mass spectrometer at the CSIRO radiogenic isotope facility in Sydney. External precision of ± 0.000018 (2 standard errors of the mean) is assumed from measurement of the NBS 987 standard over the period of analysis. Strontium isotope ages were determined from the seawater strontium curve of McArthur et al., (2001) using Look-up table Version 5: 09 04 12, calibrated to the GTS2012 timescale of Gradstein et al., (2012). $^{87}Sr/^{86}Sr$ ratios reported herein

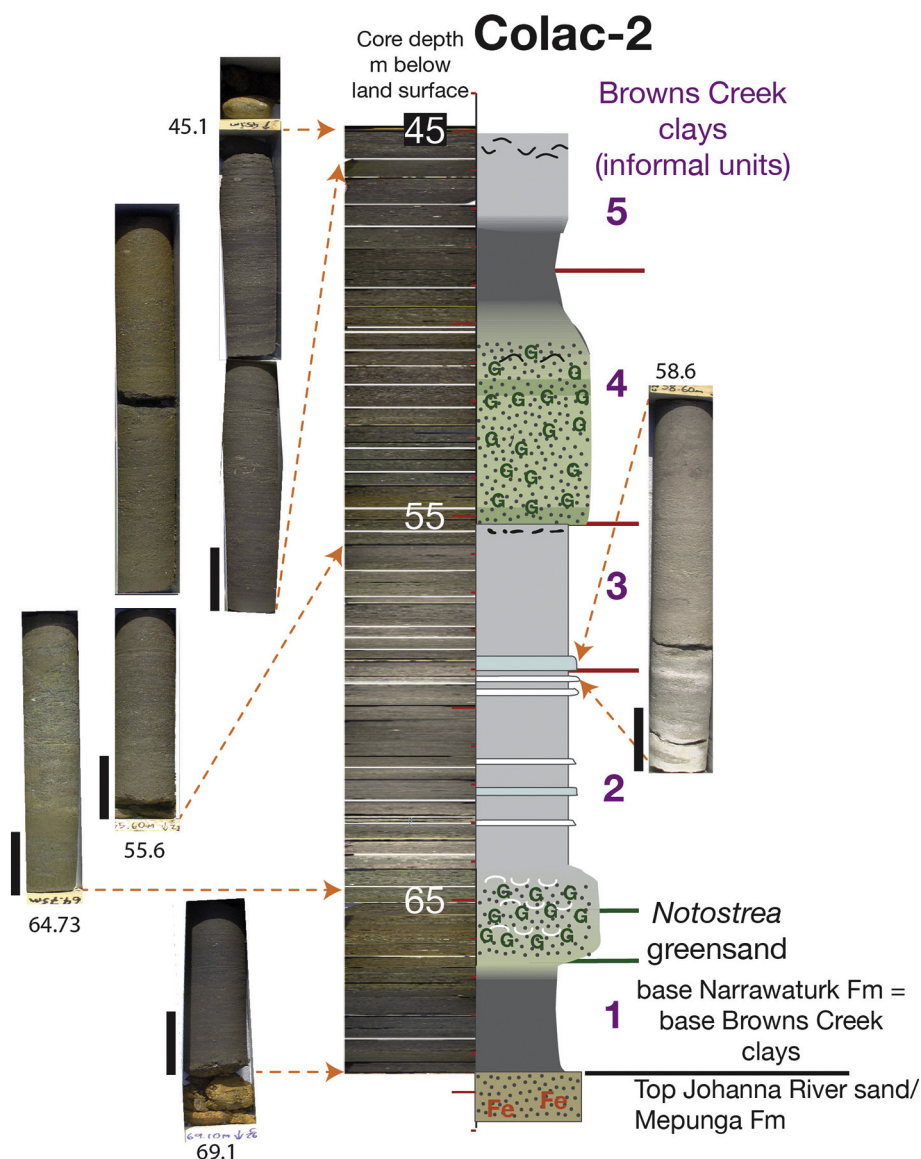**Fig. 6.** Colac-2 core. Browns Creek clays informal units are numbered 1 to 5. Sample core segments are shown with core heights (metres; black bar = 10 cm). The visual core display (VCD) next to the log was constructed from the photographed core to show facies colour variations.

(Table 2) are normalized to NBS987 $^{87}Sr/^{86}Sr = 0.710235$. The results were recalibrated to the standard NBS987 = 0.710248 (Table 3) for comparison with the Look-up tables.

Sr isotope ratios were measured on the CC brachiopods (single specimens) using a Neptune MC-ICPMS at the University of South Carolina. Samples were introduced into the MC-ICPMS by way of a high efficiency inlet system (APEX, Elemental Scientific, Omaha, NE). With the Jet Interface, consisting of the Jet-sampler and X-skimmer cones, and a 100 μl/min nebulizer instrumental sensitivity was 2400 v/ppm Sr. Isotope measurements consist of 40 cycles of 8 s. All isotopes of Sr were collected. We monitored masses 82 and 83 for krypton (Kr) to correct for interference of ^{86}Kr on mass 86. Krypton is present in trace quantities in bulk argon supply tank. The Kr correction was negligible as calculated ^{86}Kr contributed less than 0.01% to the total signal on mass 86. We also monitored mass 85 for rubidium (Rb) to correct for interference for ^{87}Rb on mass 87. Presence of Rb is indicative of inadequate separation during column chemistry. The Rb correction was negligible as ^{87}Kr contributed less than 0.001% to the total signal on mass 87. Instrumental mass fractionation was corrected by normalizing all measured ratios to a reference ratio of $^{86}Sr/^{88}Sr = 0.7219$ with an

exponential function. Results for replicate analysis of the Sr isotope standard SRM-987 (with a value of 0.710248) during this analytical session are $^{87}Sr/^{86}Sr = 0.710265 \pm 0.000010$ (2σ, $n = 6$). All CC values were adjusted to the SRM-987 standard.

4. Results

4.1. Facies and stratigraphy

The succession can be subdivided into the two main units: Johanna River sands (Mepunga Formation) and the Narrawaturk Formation. Several other laterally correlative units are distinguished in the Narrawaturk Formation including 5 informal units described in this work in the Browns Creek clays (Units 1 to 5) and the previously described *Notostrea* greensand and Castle Cove limestone. These are described below:

4.1.1. Johanna River sands (Mepunga formation)

The lower 2 m of BCE (Figs. 3, 7) are coarse ferruginous calcareous sand with two cemented sandy limestone (packstone/grainstone > 60%
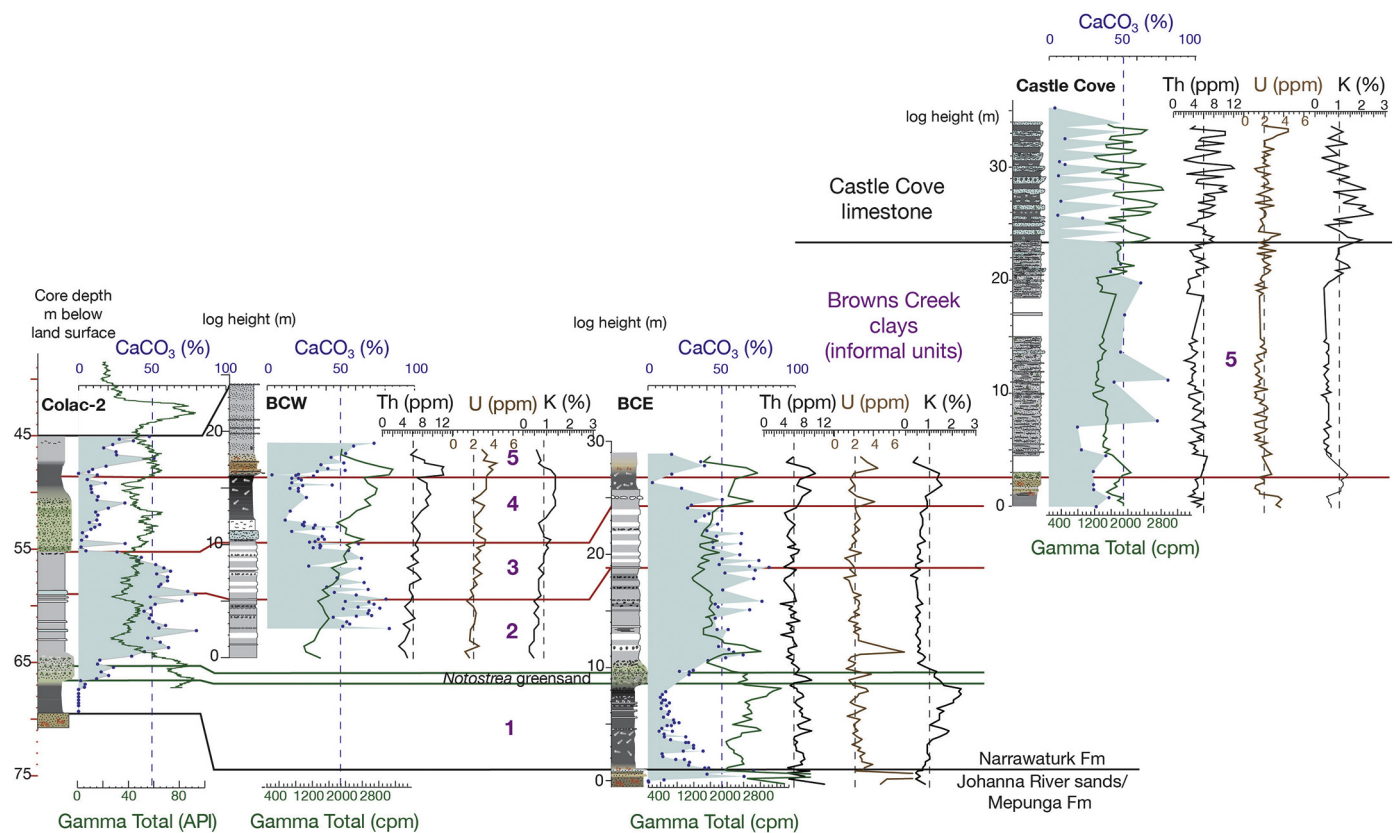
Fig. 7. A west-east correlation of Colac-2 core, Browns Creek West, Browns Creek East and Castle Cove using facies, weight %carbonate (blue graph) and downhole/outcrop gamma log data. Note: unit 4 thickens markedly westward while units 1 and 2 thin. The section is datumed on the unit 4/5 boundary; cpm = counts per minute; ppm = parts per million. (For interpretation of the references to colour in this figure legend, the reader is referred to the web version of this article.)

CaCO3) horizons. Gamma values are high > 2800 cpm with low %K, fluctuating high Th and U values. In Colac-2 the lowermost part of the core this unit is a coarse ferruginous sand.

4.1.2. Narrawaturk formation

This formation is divided into two units: Browns Creek clays and Castle Cove limestone,.

4.1.2.1. Browns Creek clays.
The lower part of this interval (unit 1, Fig. 3; 7) in BCE are seven meters of dark grey to black calcareous clay (wackestone) with common *Turritella* spp. with occasional lighter grey cemented limestone (packstone), nodular limestone and burrowed horizons with pyrite concretions in the upper half. Calcareous content decreases up section (30 to 10%) while gamma values increase from 2000 cpm (low % K < 1%) to a maximum of > 2900 cpm (high % K > 2%). Th values are relatively high > 6 ppm and fluctuating while U values remain low. Two maxima of %K at log level 4 m and 7.5 m (Fig. 7) account for the high gamma values where % carbonate is low. In Colac-2, unit 1 is a 2.5 m-thick black/dark grey clay grading upwards to a calcareous clay and gamma maximum at 66.5 m log level. This maximum correlates to a peak at 8 m log level in BCE (Fig. 7).

Unit 1 is overlain by the *Notostrea* greensand, a distinctive previously recognized unit that outcrops in BCE (Fig. 3d, 7) and subcrops in Colac-2 (Figs. 6, 7). The uppermost burrowed black high-gamma clay of unit 1 grades up section to ~2 m of coarse shelly glauconitic calcareous sand (above log level 8 m in BCE and 67 m in Colac-1). *Notostrea* spp. form a horizon at 9.5 log level in BCE yet does not form a distinct horizon in Colac-2. Gamma values decrease up section in this unit (when %K decreases from 2 to 1%) with a minor peak at 9.5 m in BCE that correlates with a maximum just below 65 m in Colac-2 (Fig. 7).

Up to 15 m of grey marl (wackestone) and light grey calcisiltite (packstone) interbeds (units 2 and 3) dominate the strata overlying the *Notostrea* greensand in BCE and BCW, these units are not as distinctive in the Colac-2 section (Figs. 3, 4, 7) but can be correlated based on gamma and %carbonate. With the exception of a horizon with high gamma (U ppm) values at ~11.5 m in BCE, values are low compared to the overlying and underlying units (< 2000 ppm with low %K < 1% and Th ppm in outcrop and < 60 API in Colac-2, Fig. 7). Alternations of grey marl and dark grey clayey marl (wackestone) typify unit 2 with minor 0.5 m thick light-grey calcisiltite (packstone) beds (near the base) and concretionary (nodular) horizons. The base of unit 3 (log level 19 m BCE, 5 m BCW (Fig. 4) and 59.5 m in Colac 2) and top of unit 2 is a 10 cm thick limestone (packstone/grainstone) with > 80% carbonate (this distinctive thin laterally correlative limestone records the maximum %carbonate for the section just above a gamma-poor interval). Overlying this are distinct metre-scale alternations of light grey calcisiltite (packstone)/grey marl (wackestone) in outcrop with occasional bioturbated horizons in BCW and BCE (Figs. 3, 4, 7). The %carbonate in Colac-2 does not vary as much as the BCE and BCW outcrop, primarily due to the presence of mainly marl (wackestone) facies with minor thin limestone (packstone/grainstone) and calcisiltite (packstone) horizons (Figs. 6, 7) however, overall the gamma patterns are similar to BCW with a gamma low at 64 m in Colac-2 equivalent to that near the base of the BCW section (Fig. 7) with another minimum below the unit 2/3 boundary that is present in BCE and BCW. Gamma values decrease up section in unit 3 while %carbonate decreases.

Unit 4 is lithologically variable however it is correlated across all sections based on its relatively low fluctuating %carbonate and similar gamma profiles (Fig. 7). The base of this unit is below a gamma maximum (U ~ 3–4 ppm) associated with a reduction %carbonate compared to unit 3 to < 40%. Calcareous glauconitic sand makes up the
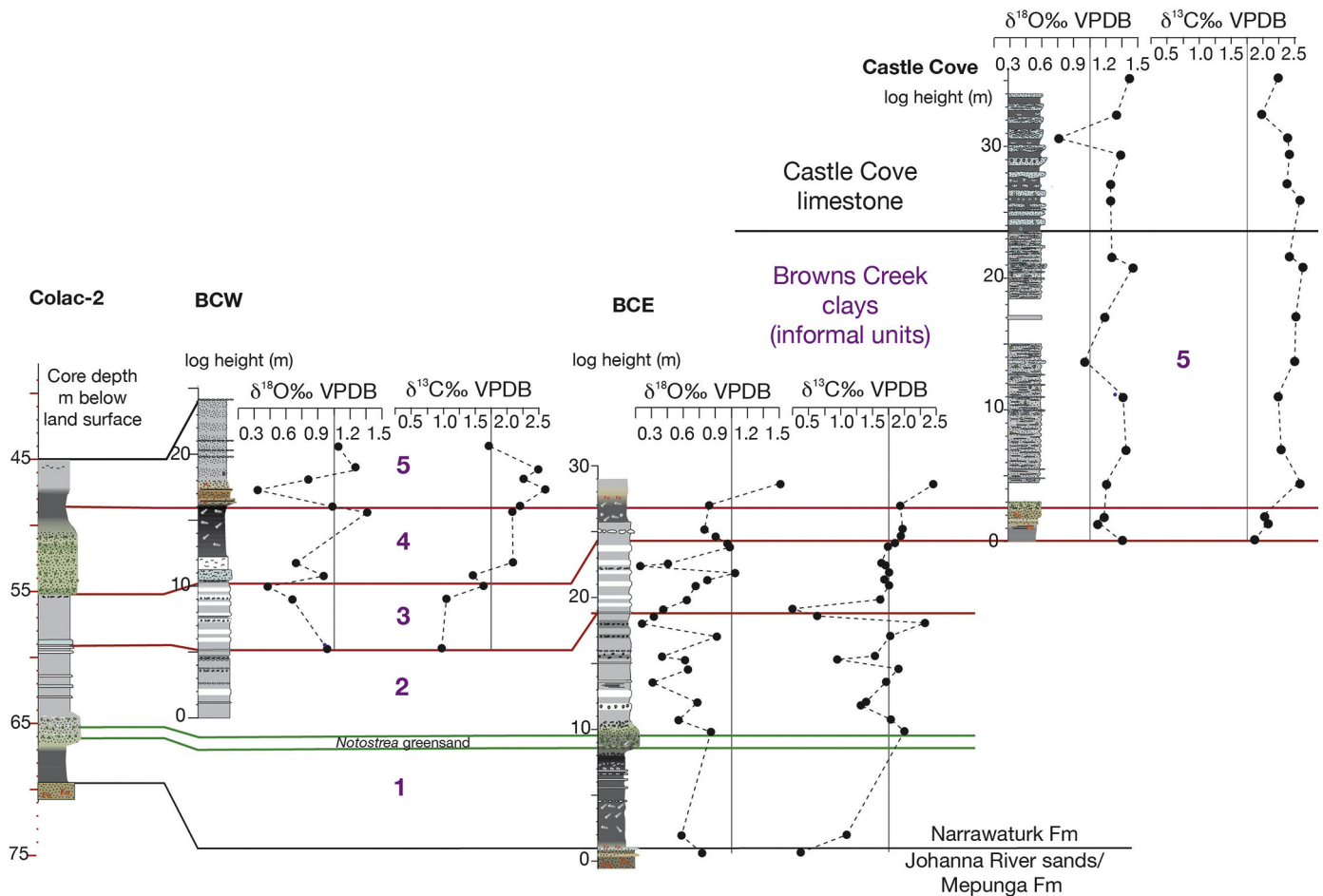
Fig. 8. Benthic foraminiferal *Cibicidoides* spp. oxygen and carbon isotope data from BCE, BCW and Castle Cove (Supplementary Table S1).

lower 5 m of this unit in Colac-2. The lower part of unit 4 in BCW is a dark grey bioturbated clayey marl (wackestone), overlain by a metre of grey shelly sandy limestone (packstone/grainstone) and a metre of light grey shelly calcisiltite (packstone). A marl (wackestone) forms the base of unit 4 in BCE and CC (Fig. 7). One to four meters of black to dark grey (*Turritella*-rich in outcrop) calcareous clay with relatively high %K (> 1%) forms the rest of unit 4 in Colac-2, BCW and BCE (Fig. 3). In CC however, the equivalent strata to this clay is a %K-rich (low gamma) glauconitic shelly calcareous sand.

Similar to unit 4, unit 5 is also lithologically variable but can be correlated based on gamma trends. A basal gamma maximum (with peaks of 1.5% K and > 10 ppm Th in outcrop) ties the sections (Fig. 7). The base of unit 5 is a clay that grades up section to marl (wackestone) in Colac-2 (Fig. 6) and BCE (with iron staining, Fig. 3). In BCW the upper bioturbated part of unit 4 is overlain by laminated and ripple cross-laminated well sorted ferruginous calcareous shelly fine sand at the base of unit 5 (Fig. 4). This is in turn overlain by ferruginous shelly sand marl (wackestone) and a layer of laminated well-sorted fine sand followed by over seven meters of grey sandy marl (wackestone) (Figs. 4, 7). In CC a basal glauconitic shelly calcareous sand is overlain (with two exposure gaps) by around 20 m of light-grey shelly sandy marl (wackestone) with thin bedded continuous and discontinuous sandy limestones (grainstones). Two of these sandy limestone horizons preserve irregular scoured bases and metre-scale low angled trough cross bedding at ~10 and ~ 21 m log level (Fig. 5). Gamma values are low in this unit associated with low Th, U and %K. The values increase in the upper three metre of unit 5.

4.1.2.2. Castle Cove limestone. The base of this unit in CC (Fig. 5) is

defined as the first brown calcareous clay in a series of metre scale cyclic alternations of brown calcareous clay (~10% CaCO3) and grey sandy limestone (grainstone). Brachiopods and bivalves are common with minor glauconite. Many of the sandy limestone units are discontinuous or have irregular scoured bases. Low angle cross bedding is common in the limestone above 29 m (Fig. 5). Gamma values fluctuate strongly with the clay predominantly gamma-rich (due to high %K and Th), however, some of the limestones also show gamma maxima near the top of some of the beds.

4.2. Benthic foraminiferal oxygen and carbon isotopes

The *Cibicidoides* spp. $\delta^{18}O_{CIB}$ values were adjusted to seawater equilibrium values by adding +0.64‰ (Shackleton and Opdyke, 1973). All other values were not adjusted. $\delta^{18}O_{CIB}$ values are light (< 0.9‰) in units 1 and 2 (Fig. 8) reaching maximum of ~1‰ at around 10 and 17 m log level in BCE. $\delta^{13}C_{CIB}$ values fluctuate increasing from < 0.9‰ near the base of BCE to > 1.75‰ at ~10 m with variable values above this level in unit 2. $\delta^{18}O_{CIB}$ and $\delta^{13}C_{CIB}$ values generally become more positive up section in unit 3 in BCE, with an interval of more negative $\delta^{18}O_{CIB}$ values at ~22.5 m.

$\delta^{13}C_{CIB}$ values in BCE, BCW and CC increase from < 1.75‰ to > 2.25‰ up section from units 3 to 5 and remain more positive into the Castle Cove section (Fig. 8). $\delta^{18}O_{CIB}$ values are more positive near the top of unit 4 and increase into unit 5, however, values fluctuate markedly while $\delta^{13}C_{CIB}$ values remain stable. $\delta^{18}O_{CIB}$ values are generally more positive > 1.05‰ in units 5 and the Castle Cove limestone in CC with minor fluctuations.
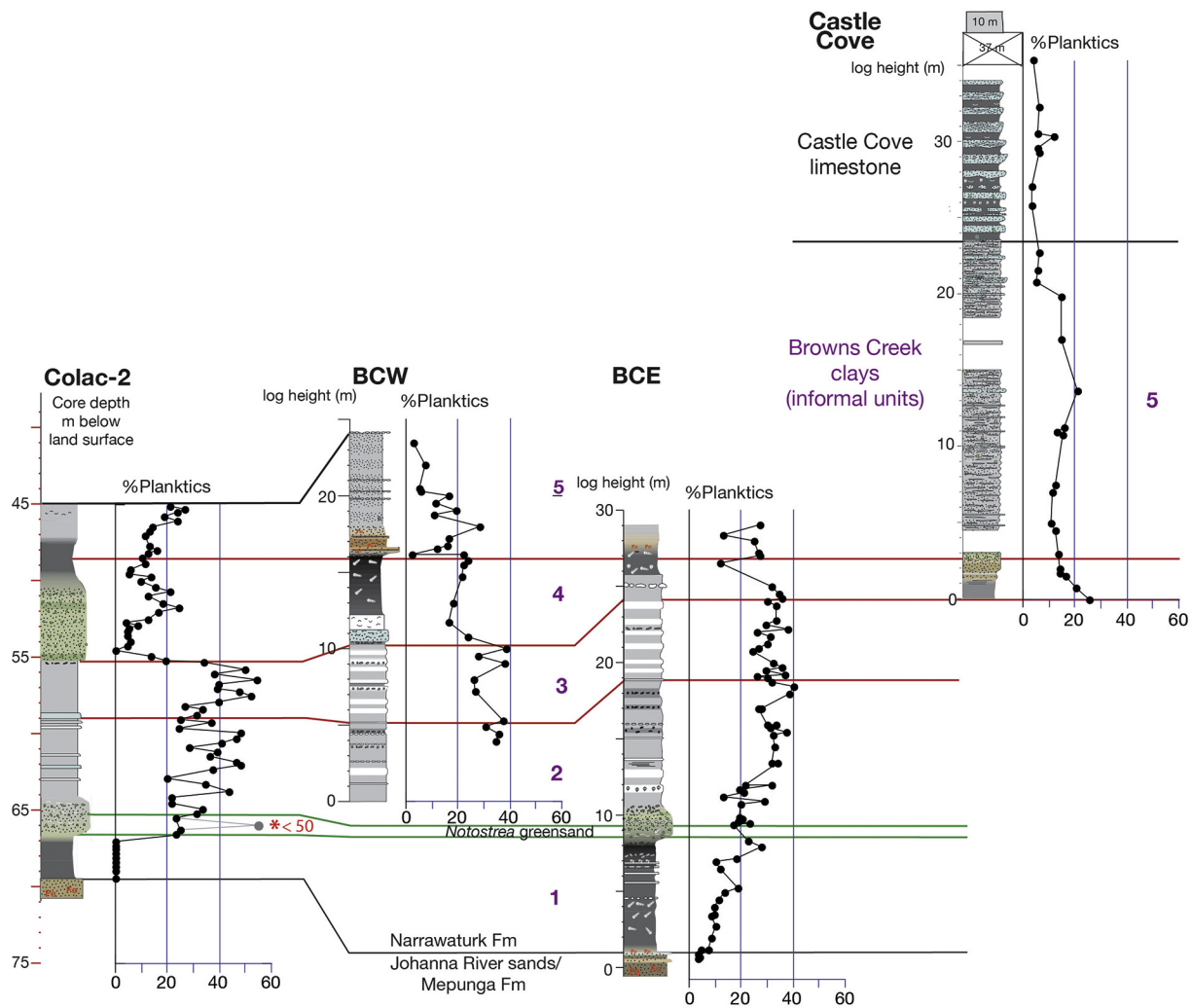
Fig. 9. The percentage planktics in the total foraminiferal assemblages in Colac-2. BCE, BCW and Castle Cove (Supplementary Table S1). The asterisk in Colac-2 denotes an horizon where < 50 foraminifera were counted.

4.3. %Planktic foraminifera

The %planktic foraminifera in the total assemblage varies along strike and up section (Fig. 9; Supplementary Table S1). Foraminifera are absent in Johanna River Sands (Mepunga Fm) and unit 1 of the Browns Creek clays in Colac-2. %Planktics increase in abundance up section from ~5% Johanna River Sands (Mepunga Fm) to ~28% in unit 1 in the BCE. Planktics are relatively common in the *Notostrea* greensand (22–30%). In unit 2 the %planktics increase from ~20% near the base to ~50% near the top in Colac-2 and 35–40% in BCW and BCE, although values fluctuate markedly in Colac-2 in this interval (generally > 20% to 50%). %Planktics is reduces at the unit 2/3 boundary to ~30% followed up section in unit 3 by variable yet higher planktic percentages (up to ~50%) in Colac-2 and BCW and BCE (up to ~38%). With exception of the basal unit in BCW and CC (~35%) the %planktics in all sections reduces to ~20% or less in unit 4 (Fig. 9). In the overlying unit 5%planktics fluctuate markedly along strike with occasional maxima of ~30% yet generally staying less than 20%. The %Planktics are less than ~10% in the upper part of unit 5 and into the Castle Cove limestone (Fig. 9).

4.4. Biostratigraphy

We describe palaeontologic data from each section and combine this with previous data (Shafik, 1981; Shafik, 1995; Waghorn, 1989; Abele,

1994) to determine the biostratigraphic framework (Figs. 10, 11, Supplementary Table S1).

4.4.1. Foraminifera

This section focusses on the distribution of biostratigraphically significant foraminiferal taxa (Fig. 10). The top of *Acarinina collactea* and *A. primitiva* is at 1.5 m log level in BCE (Abele, 1994), at the same level previously reported by McGowran (1978, 2009). The top of these taxa is also at 67 m in Colac-2. *Hantkenina compressa* is rare and confined to the *Notostrea* greensand in BCE. *Globigerinatheka index* is common in most samples in BCE, BCW and CC and its last rare occurrence is near the top of the Castle Cove limestone (McGowran, 1978) above its last common occurrence at the base of the Castle Cove limestone in CC (Abele, 1994). The top common *G. index* is just below 55 m in Colac-2, above this it is rare to 45 m log level. Similar to *G. index*, *Tenuitella insolita* is present where it last occurs in unit 5. Its top common occurrence is near the base of unit 5 in BCE and CC. The base of *Sphaeroidina* spp. is in the late Eocene in the St. Vincent Basin (700 km northwest of Browns Creek) and has previously been documented in the top 5 m of BCE (McGowran et al., 1992). Our data confirms this, as the base of this taxon is near the top of unit 4 in Colac-2, BCE and BCW and is present at the base of CC (Fig. 10). This benthic foraminiferal datum enhances the correlation of the 5/4 unit boundary between the four sections (Fig. 7). The top of common *Pseudohastigerina micra* is at 56.4 m in Colac-2, at ~25 m log level in BCE (McGowran,
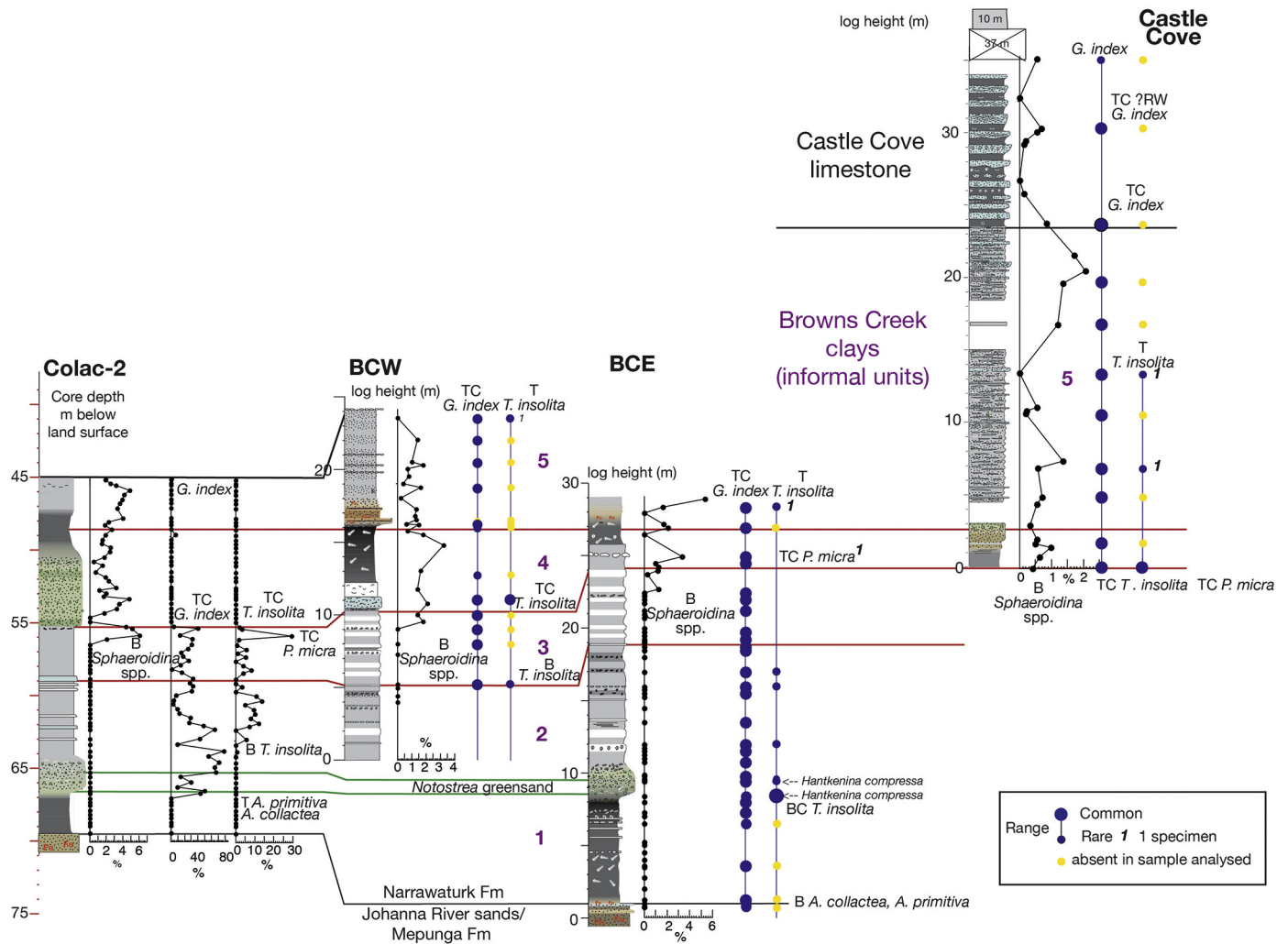
Fig. 10. Foraminiferal biostratigraphic data (see text for details; Supplementary Table S1). %*Sphaeroidina* spp. is expressed as a percentage of the benthic rotaliid foraminifera. The %*Globigerinatheka index* and %*Tenuitella insolita* in Colac-2 are plotted as a percentage of the total planktic foraminifera. T = top; TC = top common; B = base; BC = base common. Semi-quantitative data are round circles. Nannofossil datums have green lettering whereas foraminiferal datums have black lettering. RW = reworked. [1]The BC of *Pseudohastigerina micra* in BCE is from McGowran (1987). (For interpretation of the references to colour in this figure legend, the reader is referred to the web version of this article.)

1978) and at the base of CC (Abele, 1994).

4.4.2. Nannofossils

The assemblages in the twenty-four samples analysed are diverse and attain species richness values (up to 66 species) that are higher than is typically observed in coeval Paleogene sections (Bown et al., 2004). The high quality of preservation is evident from the presence of abundant small coccoliths (*Reticulofenestra* spp. and small coccolithaceans) and conspicuous fragile taxa, such as holococcoliths and fragile *Blackites* and *Rhabdosphaera* spp. The assemblages are dominated by reticulofenestrids alongside common *Blackites* spp. and frequent to common *Coccolithus pelagicus*, *Isthmolithus recurvus*, *Pontosphaera* spp. and the holococcoliths species *Lanternithus minutus* and *Zygrhablithus bigugatus*.

The base of BCE (Fig. 11) includes rare *Ismolithus recurvus* as previously reported by Shafik (1981, 1995) and the presence of *Chiasmolithus oamaruensis*. The base common *I. recurvus* is at 7.25 m (BCE) followed by the top of small *Reticulofenestra reticulata* at 8 m (see also Shafik, 1981, 1995). The top of *Discoaster saipanensis* is at ~19 m in BCE, ~ 56 m in Colac-2 and at the base of CC (Waghorn, 1989) but is almost always very rare. The top common *Chiasmolithus oamaruensis* is at 28.4 m in BCE. The top common *Clausiococcus subdistichus* is at

~30 m in CC in the Castle Cove limestone. The top of *Pontosphaera pulchra* and *Coccolithus formosus* are above the 30 m log level of CC (Fig. 11).

4.4.3. Palynomorphs

4.4.3.1. Dinoflagellates.
At Browns Creek, dinocyst assemblages are rich and very well preserved. *Enneadocysta pectiniformis* occurs as the mid-low latitude counterpart species of *E. diktyostila* and specimens of *Deflandrea* primarily constitute *Deflandrea phosphoritica*. Assemblages are dominated by *Spiniferites* spp., a generalist cosmopolitan taxon (Sluijs et al., 2005). The low-latitude taxa *Schematophora speciosa* and *Hemiplaciphora semilunifera* are abundant to dominant in unit 1 below the *Notostrea* Greensand (Fig. 11). Unit 3 is characterized by typical outer neritic taxa (*Spiniferites* spp., *Operculodinium* spp.). The first occurrence of *Stoveracysta kakanuiensis* is at the base of unit 5 in BCW and is present with *Reticulatosphaera actinocoronata* until log level 20.5 m (Fig. 11).

4.4.3.2. Spores/pollen.
Samples from log level 7.5 to 20 m in BCW are assigned to the late Eocene Middle *Nothofagidites asperus* spore-pollen Zone (Fig. 11) based on the presence of *Anacolosidites sectus* and *Tricolpites magnificus* (Partridge, 1999). The top of *Aglaoreidia*
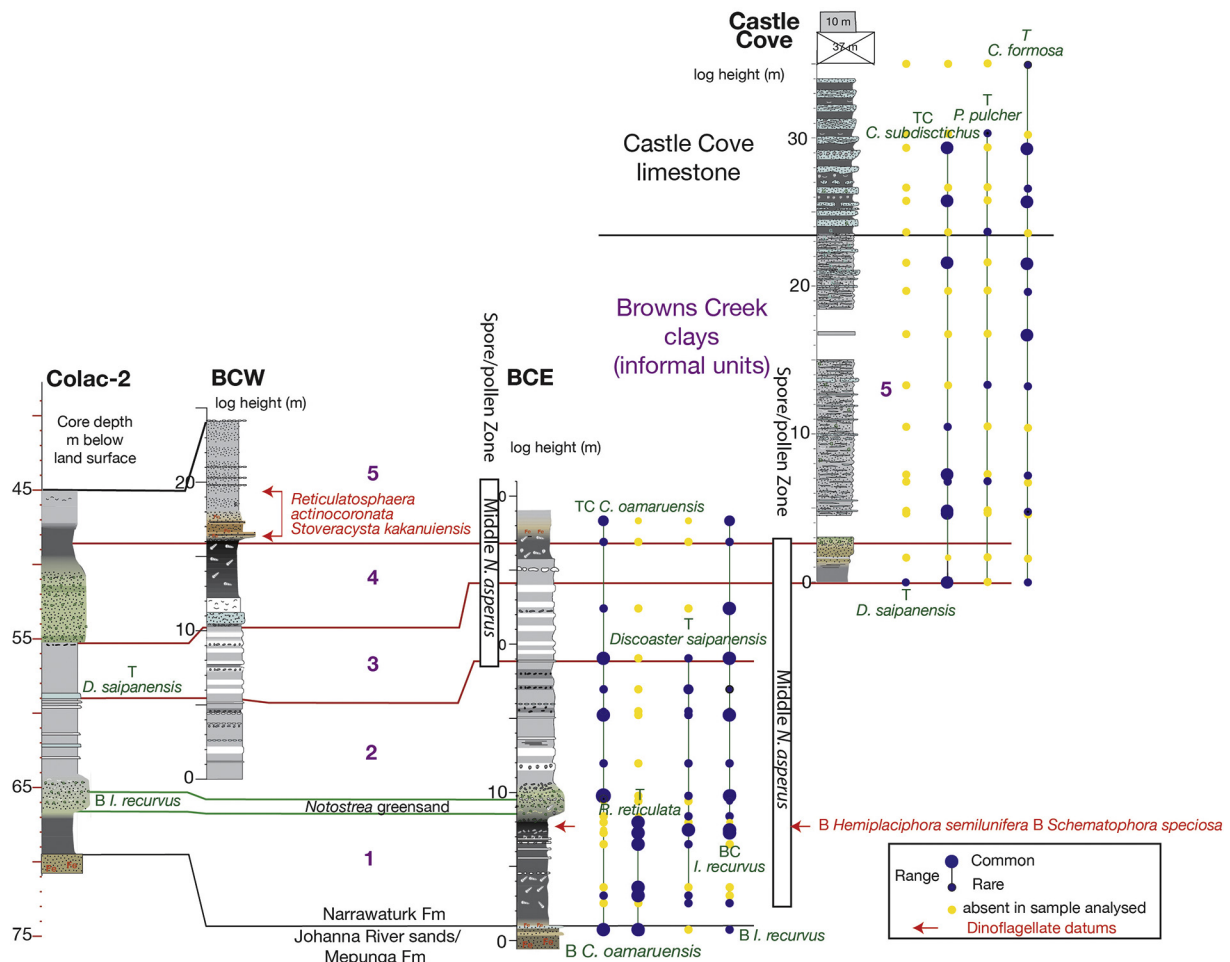
12

Fig. 11. Nannofossil and organic microfossil biostratigraphic data (see text for details; Supplementary Table S1). T = top; TC = top common; B = base; BC = base common. Semi-quantitative data are round circles. Nannofossil datums have green lettering, dinoflagellate datums are red and the spore-pollen zonation is black. (For interpretation of the references to colour in this figure legend, the reader is referred to the web version of this article.)

qualumis (Stover and Partridge, 1973) and *Proteacidites stipplatus* is in the upper part of the section confirming a Middle *N. asperus* spore-pollen Zonal age (Partridge, 1999). The presence of *Proteacidites pachypolus*, *Proteacidites leightonii*, *Proteacidites crassus* and *Santalumidites cainozoicus*, which last appear in the Middle *N. asperus* spore-pollen Zone (Partridge, 1999), is consistent with the zone assigned, in the absence of younger zonal indices (i.e., *Granodiporites nebulosus* and *Foveotrilites crater*).

Log level 2 to 27 m in BCE is also assigned to the Middle *Nothofagidites asperus* spore-pollen Zone (Fig. 11) based on the presence of *Aglaoreidia qualumis* and of *Tricolpites magnificus* and *Anacolosidites sectus* (Partridge, 1999). This is supported by the presence of *Proteacidites stipplatus* in the upper part of BCE, with *Proteacidites pachypolus*, *Proteacidites leightonii* and *Proteacidites crassus*, which last appear in the Middle *N. asperus* spore-pollen Zone (Partridge, 1999). A lack of indicators from younger zones (i.e., *Granodiporites nebulosus* and *Foveotrilites crater*) is consistent with the zone assigned.

Samples from the lower metre in CC are also assigned to the late Eocene Middle *Nothofagidites asperus* spore-pollen Zone based on the presence of *Proteacidites stipplatus* Partridge in Stover and Partridge, 1973, which first appears in the upper part of this zone (Partridge, 1999). The presence of *Tricolpites thomasii*, *Proteacidites pachypolus* and *Proteacidites leightonii*, which last appear in the Middle *N. asperus* spore-pollen Zone (Partridge, 1999) is consistent with the zone assigned in the absence of indicators from younger zones.

4.5. Brachiopod strontium isotope chronology

The strontium isotope age estimates of the three horizons of brachiopods in the *Notostrea* greensand have wide error ranges from 34.5 to > 38 Ma (Fig. 12). However, the preferred age range of each horizon (two brachiopods analysed) from 8 to 8.5 m is very similar (36.74 ± 2.21 Ma). The replicate analyses of the four brachiopods at 9.5 m (the *Notostrea* horizon) is better constrained (36.72 + 1.34/ −1.22 Ma). The next sample in BCE at 18 m also has a large age error with a preferred age from 35.47 + 3.38/−1.26 Ma. The two sets of brachiopod samples from 25 and 26 m in BCE yield similar ages of 34.27 + 1.37/−0.78 Ma and 34.29 + 0.55/−0.43 Ma (replicate analyses of six brachiopods). Two brachiopods near the base of the CC (2.25 m) yield well constrained ages of 34.1 + 0.15/−0.16 and 34.19 ± 0.15 Ma. These are followed up section by brachiopod ages of 34.4 + 0.18/−0.16 Ma (log level 10 m) and 34.05 + 0.15/−0.16 Ma (log level 20.5 m) suggesting the uppermost part of the Brown Creek clays is latest Eocene to earliest Oligocene in age. The Castle Cove limestone (Fig. 10) yields early Oligocene ages of 33.79 ± 0.17 Ma (log level 27 m), 33.63 + 0.17/−0.16 Ma (log level 30.25 m) and 33.72 + 0.17/−0.16 Ma (log level 32.25 m). An uppermost brachiopods sample 47 m above the last outcrop of Castle Cove limestone yields an age of 32.9 + 0.15/−0.18 Ma age (Fig. 12).
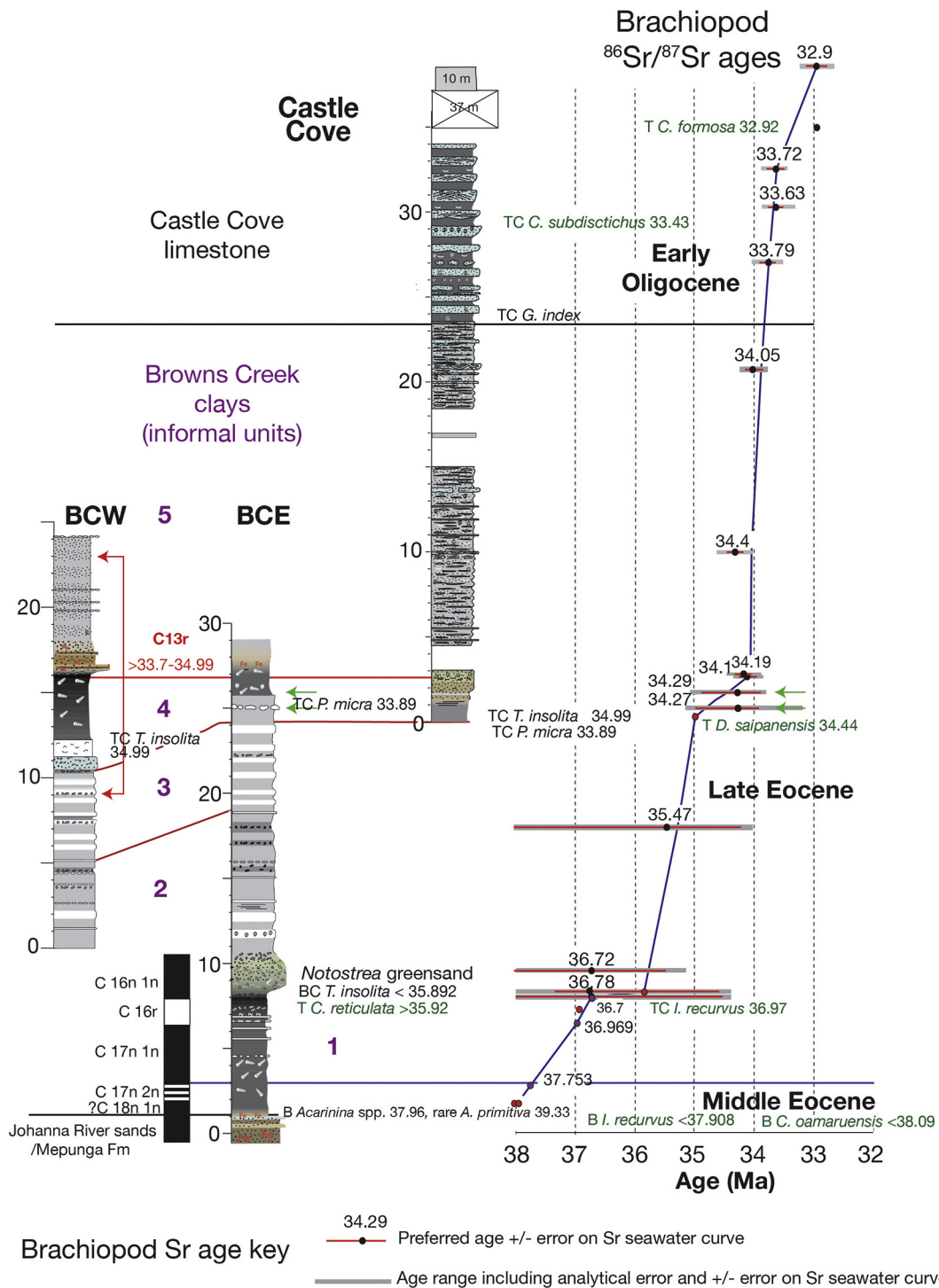
Fig. 12. A composite section of Browns Creek West, East and Castle Cove with microfossil datums and their GTS2012 (Gradstein et al., 2012) biochronology. The magnetostratigraphy of the lower 10 m BCW is from Shafik and Idnurm (1997) and McGowran (2009). Brachiopod $^{86}Sr/^{87}Sr$ preferred age and age ranges derived from McArthur et al., (2001) calibrated to GTS2012 (Tables 1, 2 and 3). The green arrows are two brachiopod Sr isotope dates from near the top of BCE. The chronology of the dinoflagellate datums in BCW is in red. (For interpretation of the references to colour in this figure legend, the reader is referred to the web version of this article.)

5. Discussion

Integrated bio/chronostratigraphic analyses of a high paleolatitude (55°S) Paleogene section in southeast Australia shows that the sections range in age from the middle Eocene to the early Oligocene. The strata in this area are typical neritic facies deposited at palaeodepths less than 100 m on a cool-water carbonate ramp (Boreen and James, 1995;

Gallagher and Holdgate, 2000; Gallagher et al., 1999). We discuss facies and the chronological framework of the section below and its likely relationship to global Eocene/Oligocene boundary events.

5.1. Facies and palaeodepth

The cyclic alternations of marl (wackestone)/calcareous clay and

Table 2
The age of the brachiopods in BCE (Fig. 10).

Sample ID	BCE log ht. m	87Sr/86Sr	2 s error	Age Range (Ma)	Preferred age (Ma)	n
B8	8	0.707755	0.000010	37.45–34.58	36.46 + 0.29/−1.51	2
B8.5	8.5	0.707755	0.000010	37.45–34.67	36.46 + 0.29/−1.42	2
B9.5	9.5	0.707755	0.000009	37.45–35.33	36.46 + 0.29/−0.53	4
B18	18	0.707772	0.000011	36.00–34.05	35.23 + 0.22/−0.99	2
B25	25	0.707808	0.000009	34.45–33.48	33.97 + 0.31/−0.34	2
B26	26	0.707807	0.000009	34.45–33.73	33.99 + 0.31/−0.12	6

Note: measured isotopic ratios normalized to the standard SRM987 = 0.710248. External Precision from measurement of NBS987standard ± 0.0020% (± 0.000018) (95% confidence limits). Ages calculated from McArthur et al. (2001). Preferred ages include the error on the Sr sea-water curve from the Look-up table Version 5: 09 04 12, calibrated to the GTS2012 timescale of (Gradstein et al., 2012). Age range includes the errors of the look up table and analytical error.

Table 3
The age of the brachiopods in CC (Fig. 10).

Sample ID	CC log ht. m	87Sr/86Sr	2 s error	Age range (Ma)	Preferred age (Ma)	n
CC2.25	2.25	0.707817	0.000006	34.47–33.73	34.10 + 0.15/−0.16	1
CC2.25×	2.25	0.707812	0.000008	34.57–33.82	34.19 + 0.15/−0.15	1
CC10M	10	0.707802	0.000008	34.91–34.04	34.40 + 0.18/−0.16	1
CC01	20.5	0.707820	0.000005	34.41–33.67	34.05 + 0.15/−0.16	1
CC04	27	0.707832	0.000007	34.15–33.42	33.79 + 0.17/−0.17	1
CC05	30.25	0.707840	0.000005	34.01–33.28	33.63 + 0.17/−0.16	1
CC06	32.25	0.707836	0.000005	34.09–33.36	33.72 + 0.17/−0.16	1
A20	82	0.707880	0.000006	33.23–32.48	32.90 + 0.15/−0.18	1

Note: Instrumental mass fractionation was corrected by normalizing all measured ratios to a reference ratio of $^{86}Sr/^{88}Sr$ = 0.7219 with an exponential function. Results for replicate analysis of the Sr isotope standard SRM-987 (with values 0.710248) during this analytical session are $^{87}Sr/^{86}Sr$ = 0.710265 ± 0.000010 (2σ, n = 6). All CC values were adjusted to the SRM-987 standard. Ages calculated from McArthur et al. (2001). Preferred ages include the error on the Sr sea-water curve from the Look-up table Version 5: 09 04 12, calibrated to the GTS2012 timescale of (Gradstein et al., 2012). Age range includes the errors of the look up table and analytical error.

packstone cycles in the Browns Creek section have been interpreted to have been deposited in a deep ramp setting (Boreen and James, 1995) in middle to outer neritic environments (Shafik, 1983). These are terrigenous dilution cycles where carbonate-rich facies are interpreted to represent deeper conditions than the shallower more siliciclastic-rich facies (Boreen and James, 1995). However, the facies interpretation of Boreen and James (1995) and Shafik, 1983) only apply to informal units 2 and 3 of the Browns Creek clays and not to the siliciclastic dominated units 1, 4 and 5. The relatively high percentage planktic foraminifera in units 2 and 3 compared to units 1, 4 and 5 suggests increased oceanicity and relative palaeodepth (cf. van der Zwaan et al., 1990, 1999) where the %planktics (30–50%) represent palaeodepths ranging from 100 to 200 m (outer shelf or ramp conditions). The upward increase in %planktics and carbonates in unit 1 is interpreted to reflect deepening from the middle to late Eocene, where the basal Narrawaturk Formation (Browns Creek clays) transgressed over coarser higher energy inner to middle shelf Mepunga Formation (as previously documented regionally in the Otway Basin by Gallagher and Holdgate, 2000).

The lithostratigraphy and biostratigraphy of the sections suggests there are two erosional horizons representing gaps in the section. For example, the lower boundary of the *Notostrea* greensand is interpreted to be erosive, as a least 5 m of unit 1 is missing in Colac-2 compared to BCE. In addition, the large gamma peak (high %K) at this boundary is likely related to non-deposition followed by a condensed sequence dominated by glaucony (cf. Banerjee et al., 2016). After this deepening to middle-outer neritic depths led to the deposition of planktic- and carbonate-rich cyclic ramp facies of unit 2 and 3. The metre-scale cycles in this interval are dilution cycles where increased siliciclastic input during lower sea levels led to calcareous mud/muddy marl (wackestone) deposition and carbonate-rich siltstones (packstones) during higher sea levels (Boreen and James, 1995). The laterally variably siliciclastic-dominated facies of the overlying unit 4 is associated with a marked decrease in %planktics (to < 20%, inner to middle shelf palaeodepths cf. van der Zwaan et al., 1990, 1999), and is therefore

interpreted to have been deposited in shallower neritic conditions landward of the underlying unit 3. These strata are in turn overlain by unit 5 which is typified by a large gamma maximum with variable % planktics (generally less than %20) associated with high %K with some glaucony near the base of CC. We interpret this as a condensed horizon associated with a gap in the sequence. It is also possible that it may have been subaerially exposed leading to ferrugenization of the surface. The top of unit 3 is seven meters below the base of unit 5 in Colac-2 and BCW whereas it is 3 m below this horizon in BCE. This suggests that units 3 and 4 are tilted to the west and the erosive base of unit 5 is a low angle unconformity. The overlying facies of unit 5 is variable yet carbonate-rich (sandy well-bedded marls/wackestones) suggesting a return to slightly deeper neritic conditions (middle shelf ~20% planktics) alternating with shallow inner shelf palaeodepths (< 10% planktics) in a storm dominated ramp in the upper part of the Browns Creek clays (Boreen and James, 1995). This is overlain in turn by the distinctive calcareous clay/sandy limestone (cross-bedded and massive grainstones, Fig. 3) shallowing upward cycles in the Castle Cove limestone with less than 10% planktics interpreted to represent inner shelf tempestite cycles (Boreen and James, 1995).

5.2. Chronostratigraphic framework

We combine calcareous and organic microfossil biochrononology calibrated to GTS2012 (Gradstein et al., 2012) with brachiopod Sr isotope isotope data and benthic foraminiferal isotopes to constrain the age of the section (Figs. 10, 11, 12, 13).

(i) Middle Eocene: the basal 3.5 m of BCW and Colac-2 yield middle Eocene foraminifera: *Acarinina* spp. (T 37.96 Ma) and rare *A. primitiva* (T 39.33 Ma). Nannofossils include: rare *Ismolithus recurvus* (B 36.97 Ma) reported herein by Shafik (1981, 1983) and *Chiasmolithus oamuerensis* (B 38.09 Ma, Fig. 11). Waghorn (1989) did not observe *I. recurvus* in this interval, instead recorded it further up section near the top of unit 1. However, *I. recurvus* is also
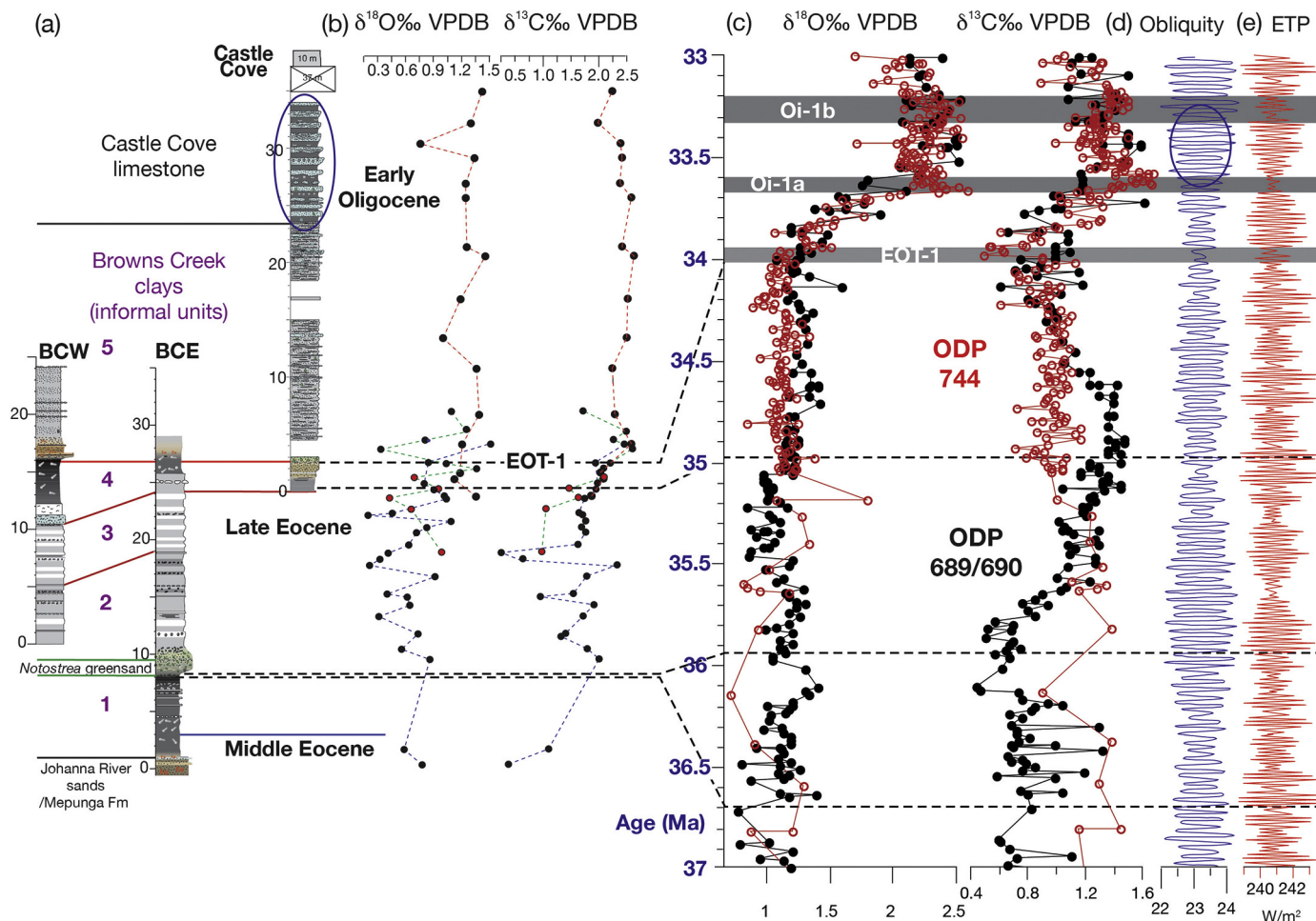
Fig. 13. A correlation of the Browns Creek and Castle Cove section chronology (from Fig. 12) with deep water southern high latitude section at OPD Sites 689/690 and 744. (a) Browns Creek West, East and Castle Cove stratigraphy (b) Composite C/O *Cibicidoides* spp. isotope data from Fig. 8. Note: five data points from unit 3 (red dots) from BCW are moved up section by 4 m. (c) Stable isotope data from ODP Sites 689/690 (Diester-Haass and Zahn, 1996) and Site 744 (Zachos et al., 1996) and from Cramer et al. (2009) recalibrated to GTS2012. (d) Obliquity (Tilt°) solution from 33 to 37 million (Laskar et al., 2004) and insolation at 55°S plotted using Analyseries 2.0 (Paillard et al., 1996). (e) The ETP (eccentricity tilt precession) solution of Laskar et al. (2004) is also shown. The strata in CC in the blue ellipse are correlated to a package of high obliquity variability cycles during Oi-1. The reader is referred to Supplementary Fig. S1 which shows how this correlation was achieved. (For interpretation of the references to colour in this figure legend, the reader is referred to the web version of this article.)

reported from Chron C17n 1n (37.785–37.908 Ma) and older (Agnini et al., 2014). Thus the lower normal interval in this section likely lies in the middle Eocene C17n2n and/or? C18n1n magnetochrons (McGowran, 2009; Shafik and Idnurm, 1997) with a youngest age of 37.872 Ma. If this is the case then the specimens of *A. primitiva* may be reworked as postulated by Abele (1994) and the middle/upper Eocene boundary is at ~3 m log level.

(ii) Late Eocene: The top of *Reticulofenestra reticulata* (T 35.92 Ma) overlapping with the base common *Ismolithus recurvus* (B 36.97 Ma) near the top of unit 1 (Fig. 11) suggests that the distinct reversal event identified by Shafik and Idnurm (1997) in this interval is likely to be C16r (36.7–36.986 Ma). The Sr dates in the overlying *Notostrea* greensand have wide preferred age errors (Fig. 12) that overlap with these biostratigraphic datums. This section also contains the base and top of *Hantkenina compressa* (T 33.89 Ma; Figs. 10, 12) and the base (common) *Tenuitella insolita* (B 35.892 Ma). These dates and the discordant stratigraphy between Colac-2 and BCW (discussed above) suggest the hiatus beneath the *Notostrea* greensand spans 35.892 to 36.7 Ma (Fig. 13) and that the normal chron event at this horizon may be C16n1n (35.706–35.892 Ma). Chronological constraints in unit 2 are sparse

and include a large error Sr brachiopod date at 18 m. Useful biostratigraphic datums above this level are present near the base of unit 4 (Fig. 12) and include the top of *Discoaster saipanensis* (T 34.44 Ma), the top of common *Pseudohastigerina micra* (TC 33.89 Ma) and the top (common) of *Tenuitella insolita* (T 34.99 Ma). Other single occurrences of *T. insolita* above this level are interpreted to be reworked (Abele, 1994). These datums lie within the preferred age ranges of the brachiopod Sr dates at this level (Fig. 12). The biochronological data suggests that the base of unit 4 is ~35 Ma (Figs. 12, 13). Strontium isotope dates above the unconformity in unit 5 have relatively reduced preferred age error ranges compared with those in units 3 to 4, with samples from Castle Cove log level 2.5 m yielding a preferred age range from 33.94–34.34 Ma. The dinocysts *Stoveracysta kakanuiensis* and *Reticulatosphaera actinocoronata* are present near the base of unit 5 (Fig. 11) and these dinocyst taxa are confined to the C13r chron (33.7–34.99 Ma; Houben et al., 2019a). In addition, there is a 0.5‰ shift to more positive $\delta^{13}C$ benthic foraminiferal isotope values in the transition from units 4 to 5 in three sections (BCW, BCE and CC, Figs. 8, 13), which is similar in magnitude to the shift at ODP Sites 689/690 and 744 associated with the EOT-1 (Eocene/

Oligocene Transition) to Oi-1 glacial transition from 34 to 33.7 Ma (Fig. 13). Therefore, combined biochronological and isotope data suggest the base of unit 5 is significantly younger than the top of unit 4 (i.e. unit 5 lies above an unconformity) and that the EOT-1 (sensu Katz et al., 2008, Coxall and Wilson, 2011; Houben et al., 2019b; ~34 Ma) is near the base of unit 5 (Fig. 13). After EOT-1 the remainder of unit 5 Sr isotope ages are ~34 Ma suggesting high sedimentation rates while $\delta^{18}O$ and $\delta^{13}C$ benthic foraminiferal isotopes fluctuate but remain positive compared to prior to the EOT-1 (Fig. 13).

(iii) Early Oligocene: All brachiopod Sr dates in the Castle Cove limestone suggest an early Oligocene age (Fig. 12). This is corroborated by the relatively positive C/O benthic isotopes (compared to the underlying Eocene) and the top common *Classicoccus subdistichus* (34.43 Ma) and the top of *Coccolithus formosus* (32.92 Ma). We suggest that the earliest Oligocene tempestite cycles in the Castle Cove are likely a manifestation of obliquity-dominated (41 kyr) sea level variability that persisted during the Early Oligocene Glacial Maximum (Pälike et al., 2006) and therefore that these strata were deposited from ~33.5 to 33.2 Ma (Fig. 13).

Common *Globigerinatheka index* (a typically Eocene planktic foraminiferal taxon) last occurs at the base of the Oligocene Castle Cove limestone with limited (reworked?) occurrences above this level (Figs. 10, 12). However, in the Austral realm the top of *G. index* is at 34.61 Ma defining the top of the AE10 Zone (Huber and Quillevere, 2005). This biochronological discrepancy has been noted in the Castle Cove section previously by Kamp et al. (1990) and Waghorn (1989) who suggested this taxon locally survived into the early Oligocene Castle Cove limestone with the regional persistence of warmer shelf conditions in a kind of refugium. In New Zealand, the top of *Globigerinatheka index* has been found to lie within the Oligocene lower Whaingaroan stage (~33 Ma) by Cooper et al. (2001) who could not explain its presence. However, these authors commented on this taxon's apparent diachroneity regionally. The last *Globigerinatheka* species *G. tropicalis* extends to the top of Zone E16 (Premoli Silva et al., 2006; 33.89 Ma). Globigerinathekids are known to be diachronous, and absent in many upper Eocene tropical and subtropical sections, such as the Indian Ocean (Wade and Pearson, 2008) and US Gulf coast (Wade et al., 2012). Chrono- and biostratigraphic data from the Castle Cove section suggests that either all the *G. index* specimens in this section are either reworked or this taxon persisted in this region until 34 Ma (similar to *G. tropicalis*) and possibly until 33.7 Ma prior to Oi-1 in a shallow warm water shelfal refugium.

5.3. Glacioeustacy

The Otway Basin depositional record would be significantly impacted by eustatic sea level fluctuations, leading to changes in accommodation space and erosional unconformities. The distinct facies alterations that occurred from the middle Eocene through early Oligocene in the Otway Basin could be interpreted in terms of glacioeustatic change. Sequence stratigraphy studies have been used to address the role of ice volume versus temperature in deconvolving the oxygen isotope signal across the EOT. High-amplitude and rapid glacioeustacy has previous been suggested, with sea-level fall of ~50 m during Oi-1 (Echols et al., 2003; Vandenberghe et al., 2003; Miller et al., 2008). Upper Eocene sequence boundaries, coincident with oxygen isotope increases, indicate sea-level fall of ~40 m, signifying short-term expansion and collapse of the Antarctic icesheet (Katz et al., 2008; Miller et al., 2008).

Our reconstructed paleodepths shift from 100 to 200 m (outer shelf) in the late Eocene to inner to middle shelf palaeodepths (0–100 m) after 34 Ma across the EOT. However, in the late Eocene there are hiatuses and condensed sections at ~36 Ma, 35 Ma and just below 34 Ma. Subsequently the onset inner shelf (0–50 m) early Oligocene Castle

Cove Limestone deposition (Figs. 7 and 8) with its cyclic alternations between limestone and calcareous clay may represent obliquity dominated glacio-eustacy that dominated the Oligocene epoch (Wade and Pälike, 2004; Pälike et al., 2006). However, glacio-eustatic interpretations in the region are hindered by compressional tectonism along the southern margin of Australia across the Eocene-Oligocene boundary, as described by Mahon and Wallace (2020). Furthermore, sea level variations may be diachronous due to glacial antisiphoning at near-field sites (Gallagher et al., 2013).

6. Conclusions

We combine new bio-, chemo- and lithostratigraphic analyses of the outcrops and subsurface core (Colac-2) at high latitude Otway Basin, southwest Australia with pre-existing data to revise the stratigraphy of this section. Our work shows that the strata in this area spanned the Eocene-Oligocene boundary. Shallow marine sequences across this critical climate threshold are rare but have the potential to record the near field eustatic and oceanic consequences of Oligocene glacial expansion and contraction (Gallagher et al., 2013). During this time the region lay at a paleolatitude of at least 55°S on the northeastern margin of the Australo-Antarctic Gulf facing the evolving Southern Ocean (McGowran, 2009). Our work has confirmed that the middle/upper Eocene boundary is near the base of the section. The overlying siliciclastic Eocene strata are truncated by an unconformity (~0.8 Ma in duration) and overlain by late Eocene glauconitic sand (the *Notrostrea* greensand) deposited as a condensed sequence after 35.9 Ma. Subsequently deepening to middle to outer neritic depths deposited cyclic carbonate dominated facies. Shallowing after ~35 Ma deposited laterally variable calcareous siliciclastic facies. These strata were tilted and eroded prior to 34 Ma leading to laterally varying shallow water facies that may have been subaerially exposed during uplift and erosion. Well-constrained brachiopod strontium isotope dates and an 0.5‰ carbon isotope excursion above this unconformity suggests the top of Browns Creek and the base of Castle Cove section correlate to EOT-1. The subsequent persistence of more positive C/O isotope values above this level likely records the transition to the Oi-1 glaciation at ~33.7 Ma. The onset of distinct shallowing upward tempestite cyclicity in the Castle Cove limestone is interpreted to be a manifestation of the onset of obliquity dominated glacio-eustacy that subsequently dominated the Oligocene epoch (Pälike et al., 2006). The shallowing from outer to inner shelf palaeodepths from the late Eocene to the early Oligocene is likely related to the onset of cryosphere expansion, however, palaeodepth estimates are complicated by the onset of regional compressional tectonism at the Eocene/Oligocene boundary that caused localized tilting and an unconformity with possible antisiphoning effects in this near-field site (Gallagher et al., 2013).

Appendix A. Supplementary data

Supplementary data to this article can be found online at https://

doi.org/10.1016/j.gloplacha.2020.103218.

References

Abele, C., 1994. Late Eocene and the Eocene/Oligocene Boundary in the Aire District, Victoria. Geological Survey of Victoria, Melbourne.

Agnini, C., Fornaciari, E., Raffi, I., Catanzariti, R., Pälike, H., Backman, J., Rio, D., 2014. Biozonation and biochronology of Paleogene calcareous nannofossils from low and middle latitudes. Newsl. Stratigr. 47, 131–181.

Banerjee, S., Bansal, U., Thorat, A.V., 2016. A review on palaeogeographic implications and temporal variation in glaucony composition. J. Palaeogeogr. 5, 43–71.

Boreen, T.D., James, N.P., 1995. Stratigraphic sedimentology of Tertiary cool-water limestones, SE Australia. J. Sediment. Res. 65, 142–159.

Bown, P.R., Young, J.R., 1998. Techniques. In: Bown, P.R. (Ed.), Calcareous Nannofossil Biostratigraphy. Kluwer Academic, pp. 16–28.

Bown, P.R., Lees, J.A., Young, J.R., 2004. Calcareous nannofossil evolution and diversity through time. In: Thierstein, H.R., Young, J.R. (Eds.), Coccolithophores: From Molecular Process to Global Impact. Springer-Verlag, Berlin, pp. 481–508.

Browning, J.V., Millerand, K.G., Pak, D.K., 1996. Global implications of lower to middle Eocene sequence boundaries on the New Jersey coastal plain: the icehouse cometh. Geology 24, 639–642.

Carter, A.N., 1958. Tertiary Foraminifera from the Aire District, Victoria. Bull. Geol. Surv. Victoria 55, 1–76.

Cookson, I.C., Eisenack, A., 1965. Microplankton from the Browns Creek Clays, southwest Victoria. Proc. Royal Soc. Victoria 79, 119–131.

Cooper, R.A., Crampton, J.S., Raine, J.I., Gradstein, F.M., Morgans, H.E., Sadler, P.M., Strong, C.P., Waghorn, D., Wilson, G.J., 2001. Quantitative biostratigraphy of the Taranaki Basin, New Zealand: a deterministic and probabilistic approach. AAPG Bull. 85, 1469–1498.

Coxall, H.K., Wilson, P.A., 2011. Early Oligocene glaciation and productivity in the eastern equatorial Pacific: Insights into global carbon cycling. Paleoceanography 26, PA2221.

Cramer, B.S., Toggweiler, J.R., Wright, J.D., Katz, M.E., Miller, K.G., 2009. Ocean overturning since the late cretaceous: Inferences from a new benthic foraminiferal isotope compilation. Paleoceanography 24.

DePaolo, D.J., Ingram, B., 1985. High-resolution stratigraphy with strontium isotopes. Science 227, 938–941.

Dickinson, J., Wallace, M., Holdgate, G., Daniels, J., Gallagher, S., Thomas, L., 2001. Neogene tectonics in SE Australia: implications for petroleum systems. APPEA J. 41, 37–52.

Dickinson, J.A., Wallace, M.W., Holdgate, G.R., Gallagher, S.J., Thomas, L., 2002. Origin and timing of the Miocene-Pliocene unconformity in Southeast Australia. J. Sediment. Res. 72, 288–303.

Diester-Haass, L., Zahn, R., 1996. Eocene-Oligocene transition in the Southern Ocean: history of water mass circulation and biological productivity. Geology 24, 163–166.

Dunham, R.J., 1962. Classification of carbonate rocks according to depositional texture. In: Ham, W.E. (Ed.), Classification of Carbonate Rocks. American Association of Petroleum Geologists, pp. 108–121.

Echols, R.J., Armentrout, J.M., Root, S.A., Fearn, L.B., Cooke, J.C., Rodgers, B.K., Thompson, P.R., 2003. Sequence stratigraphy of the Eocene/Oligocene boundary interval: Southeastern Mississippi. In: Prothero, D.R., Ivany, L.C., Nesbitt, E., Nesbitt, E.R., Nesbitt, E.A. (Eds.), From Greenhouse to Icehouse: The Marine Eocene-Oligocene Transition. Columbia University Press, pp. 189–222.

Fensome, R.A., MacRae, R.A., Williams, G.L., 2008. DINOFLAJ2, version 1. In: Foundation, A.A.O.S.P (Ed.), Data Series, 1 ed. American Association of Stratigraphic Palynologists Foundation.

Frieling, J., Huurdeman, E.P., Rem, C.C.M., Donders, T.H., Pross, J., Bohaty, S.M., Holdgate, G.R., Gallagher, S.J., McGowran, B., Bijl, P.K., 2018. Identification of the Paleocene–Eocene boundary in coastal strata in the Otway Basin, Victoria, Australia. J. Micropalaeontol. 37, 317–339.

Galeotti, S., DeConto, R., Naish, T., Stocchi, P., Florindo, F., Pagani, M., Barrett, P., Bohaty, S.M., Lanci, L., David Pollard, D., Sandroni, S., Talarico, F.M., Zachos, J.C., 2016. Antarctic ice sheet variability across the Eocene-Oligocene boundary climate transition. Science 352, 76–80.

Gallagher, S.J., Holdgate, G., 2000. The palaeogeographic and palaeoenvironmental evolution of a Palaeogene mixed carbonate-siliciclastic cool-water succession in the Otway Basin, Southeast Australia. Palaeogeogr. Palaeoclimatol. Palaeoecol. 156, 19–50.

Gallagher, S.J., Jonasson, K., Holdgate, G., 1999. Foraminiferal biofacies and palaeoenvironmental evolution of an Oligo-Miocene cool-water carbonate succession in the Otway Basin, Southeast Australia. J. Micropalaeontol. 18, 143–168.

Gallagher, S.J., Villa, G., Drysdale, R.N., Wade, B.S., Scher, H., Li, Q., Wallace, M.W., Holdgate, G.R., 2013. A near field sea level record of East Antarctic Ice Sheet instability from 32 to 27 Myr. Paleoceanography 28, 1–13.

Gallagher, S.J., Fulthorpe, C.S., Bogus, K., Scientists, E., 2017. Expedition 356 summary. Proc. Int. Ocean Discov. Prog. 356, 1–43.

Gradstein, F.M., Ogg, G., Schmitz, M., 2012. The Geologic Time Scale 2012 2-Volume Set. Elsevier.

Hill, D.J., Haywood, A.M., Valdes, P.J., Francis, J.E., Lunt, D.J., Wade, B.S., Bowman, V.C., 2013. Paleogeographic controls on the onset of the Antarctic Circumpolar Current. Geophys. Res. Lett. 40, 5199–5204.

Holdgate, G.R., Gallagher, S.J., 2003. Tertiary a period of transition to marine basin environments. In: Birch, W.D. (Ed.), Geology of Victoria. Geological Society of Australia (Victoria Division), Melbourne, pp. 289–335.

Houben, A.J., Bijl, P.K., Pross, J., Bohaty, S.M., Passchier, S., Stickley, C.E., Röhl, U.,

Sugisaki, S., Tauxe, L., van de Flierdt, T., Olney, M., 2013. Reorganization of Southern Ocean plankton ecosystem at the onset of Antarctic glaciation. Science 340 (6130), 341–344.

Houben, A.J.P., Bijl, P.K., Sluijs, A., Schouten, S., Brinkhuis, H., 2019a. Late Eocene Southern ocean cooling and invigoration of circulation preconditioned Antarctica for full-scale glaciation. Geochem. Geophys. Geosyst. 20.

Houben, A.J.P., Quaijtaal, W., Wade, B.S., Schouten, S., Brinkhuis, H., 2019b. Organic-walled dinoflagellate cysts from the Eocene-Oligocene transition in the Gulf of Mexico: indicators of climate-and sea-level change during the onset of Antarctic glaciation. Newsl. Stratigr. 52, 131–154.

Huber, B.T., Quillevere, F., 2005. Revised Paleogene planktonic foraminiferal biozonation for the Austral Realm. J. Foraminifer. Res. 35, 299–314.

Kamp, P.J.J., Waghorn, D.B., Nelson, C.S., 1990. Late Eocene-early Oligocene integrated isotope stratigraphy and biostratigraphy for paleoshelf sequences in Southern Australia; paleoceanographic implications. Palaeogeogr. Palaeoclimatol. Palaeoecol. 80, 311–323.

Katz, M.E., Miller, K.G., Wright, J.D., Wade, B.S., Browning, J.V., Cramer, B.S., Rosenthal, Y., 2008. Stepwise transition from the Eocene greenhouse to the Oligocene icehouse. Nat. Geosci. 1, 329–334.

Katz, M.E., Cramer, B.S., Toggweiler, J.R., Esmay, G., Liu, C., Miller, K.G., Rosenthal, Y., Wade, B.S., Wright, J.D., 2011. Impact of Antarctic circumpolar current development on late Peleogene Ocean structure. Science 332, 1076–1079.

Kennett, J.P., 1977. Cenozoic evolution of antarctic glaciation, the circum-Antarctic Ocean, and their impact on global paleoceanography. J. Geophys. Res. 82, 3843–3860.

Korasidis, V.A., Wallace, M.W., Wagstaff, B.E., Hill, R.S., 2019. Terrestrial cooling record through the Eocene-Oligocene transition of Australia. Glob. Planet. Chang. 173, 61–72.

Laskar, J., Robutel, P., Gastineau, M., Correia, A.C.M., Levrard, B., 2004. A long term-term numerical solution for the insolation quantities of the Earth. Astron. Astrophys. 428, 261–285.

Mahon, E.M., Wallace, M.W., 2020. Cenozoic structural history of the Gippsland Basin: early Oligocene onset for compressional tectonics in SE Australia. Mar. Pet. Geol. 114, 104243.

Martini, E., 1971. Standard tertiary and quaternary calcareous nannoplankton zonation. In: Farinacci, A. (Ed.), Proceedings of the Second Planktonic Conference Roma 1970, Rome, pp. 739–777.

McArthur, J.M., Howarth, R.J., Bailey, T.R., 2001. Strontium isotope stratigraphy: LOWESS version 3. Best-fit line to the marine Sr-isotope curve for 0 to 509 Ma and accompanying look-up table for deriving numerical age. J. Geol. 109, 155–169.

McGowran, B., 1978. Early Tertiary foraminiferal biostratigraphy in southern Australia; progress report. Bull. Australia, Bur. Mineral Resour. Geol. Geophy. 192, 83–95.

McGowran, B., 1987. Late Eocene perturbation: foraminiferal biofacies and evolutionary overturn, southern Australia. Paleoceanography 2, 715–727.

McGowran, B., 2009. The Australo-Antarctic Gulf and the Auversian facies shif. In: Koeberl, C., Montanari, A. (Eds.), The Late Eocene Earth-Hothouse, Icehouse, and Impacts. Geological Society of America, Boulder, pp. 215–240.

McGowran, B., Moss, G., Beecroft, A., 1992. Late eocene and early Oligocene in Southern Australia: Local neritic signals of global oceanic changes. In: Prothero, D.R., Berggren, W.A. (Eds.), Eocene-Oligocene Climatic and Biotic Evolution. Princeton University Press, Princeton, pp. 178–201.

McLaren, S., Wallace, M., Gallagher, S.J., Dickinson, J., McAllister, A., 2009. Age constraints on Oligocene sedimentation in the Torquay Basin, southeastern Australia. Aust. J. Earth Sci. 56, 595–604.

Miller, K.G., Browning, J.V., Aubry, M.P., Wade, B.S., Katz, M.E., Kulpecz, A.A., Wright, J.D., 2008. Eocene–Oligocene global climate and sea-level changes: St. Stephens Quarry, Alabama. Geol. Soc. Am. Bull. 120 (1–2), 34–53.

Okada, H., Bukry, D., 1980. Supplementary modification and introduction of code numbers to the low-latitude coccolith biostratigraphic zonation (Bukry, 1973; 1975). Mar. Micropaleontol. 5, 321–325.

Pagani, M., Huber, M., Liu, Z.H., Bohaty, S.M., Henderiks, J., Sijp, W., DeConto, R.M., 2011. The role of carbon dioxide during the onset of Antarctic Glaciation. Science 334, 1261–1264.

Paillard, D.L., Labeyerie, L., Yiou, P., 1996. Macintosh program performs time-series analysis. Eos 77, 379.

Pälike, H., Norris, R.D., Herrle, J.O., Wilson, P.A., Coxall, H.K., Lear, C.H., Shackleton, N.J., Tripati, A.K., Wade, B.S., 2006. The heartbeat of the Oligocene climate system. Science 314, 1894–1898.

Parr, W.J., 1947. An Australian record of the foraminiferal genus Hantkenina. Proc. Royal Soc. Victoria 58, 45–47.

Partridge, A.D., 1999. Late Cretaceous to Tertiary geological Evolution of the Gippsland Basin, Victoria. La Trobe University, Melbourne, pp. 1–439 165 figs, 9 pls (unpubl.).

Pearson, P.N., Olsson, R.K., Huber, B.T., Hemleben, C., Berggren, W.A., 2006. Atlas of Eocene Planktonic Foraminifera. Cushman Foundation for Foraminiferal Research.

Pearson, P.N., Foster, G.L., Wade, B.S., 2009. Atmospheric carbon dioxide through the Eocene-Oligocene climate transition. Nature 461, 1110–1113.

Pettijohn, E.J., 1975. Sedimentary Rocks, 3rd ed. Harper and Row, New York.

Premoli Silva, I., Wade, B.S., Pearson, P.N., 2006. Taxonomy, biostratigrpahy, and phylogeny of *Globigerinatheka* and *Orbulinoides*. In: Pearson, P.N., Olsson, R.K., Huber, B.T., Hemleben, C., Berggren, W.A. (Eds.), Atlas of Eocene planktonic foraminifera. Cushman Foundation for Foraminiferal Research, pp. 169–212.

Raggatt, H.G., Crespin, I.E., 1955. Stratigraphy of tertiary rocks between Torquay and Eastern View, Victoria. Proc. Royal Soc. Victoria 53 (175–142).

Scher, H.D., Martin, E.E., 2006. Timing and climatic consequences of the opening of Drake Passage. Science 312, 428–430.

Scher, H.D., Whittaker, J.M., Williams, S.E., Latimer, J.C., Kordesch, W.E.C., Delaney, M.L., 2015. Onset of Antarctic circumpolar current 30 million years ago as Tasmanian

Gateway aligned with westerlies. Nature 523 580− +.

Shackleton, N.J., Opdyke, N.D., 1973. Oxygen isotope and paleomagnetic stratigraphy of equatorial Pacific core V28-238: oxygen isotope temperatures and ice volumes on a 105 year and 106 year scale. Quat. Res. 3, 39–55.

Shafik, S., 1981. Nannofossil biostratigraphy of the Hantkenina (foraminiferid) interval in the upper Eocene of southern Australia. BMR J. Aust. Geol. Geophys. 6, 108–116.

Shafik, S., 1983. Calcareous nannofossil biostratigraphy; an assessment of foraminiferal and sedimentation events in the Eocene of the Otway Basin, southeastern Australia. BMR J. Aust. Geol. Geophys. 8, 1–17.

Shafik, S., 1989. Some new calcareous nannofossils from upper Eocene and lower Oligocene sediments in the Otway Basin, southeastern Australia. Alcheringa 13, 1–2.

Shafik, S., 1995. Calcareous microplankton biostratigraphy of the Eocene Browns Creek clays in the Aire District, Otway Basin of southeastern Australia; an update. AGSO J. Aust. Geol. Geophys. 16, 333–344.

Shafik, S., Idnurm, M., 1997. Calcareous microplankton and polarity reversal stratigraphies of the Upper Eocene Browns Creek clays in the Otway Basin, Southeast Australia: Matching the evidence. Aust. J. Earth Sci. 44, 77–86.

Sluijs, A., Pross, J., Brinkhuis, H., 2005. From greenhouse to icehouse; organic-walled dinoflagellate cysts as paleoenvironmental indicators in the Paleogene. Earth Sci. Rev. 68, 281–315.

Sluijs, A., Brinkhuis, H., Williams, G.L., Fensome, R.A., 2009. Taxonomical revision of the Spinidinium-Vozzhennikovia group of organic walled, peridinioid dinoflagellate cysts. Rev. Palaeobot. Palynol. 154, 34–53.

Stickley, C.E., Brinkhuis, H., Schellenberg, S.A., Sluijs, A., Roehl, U., Fuller, M., Grauert, M., Huber, M., Warnaar, J., Williams, G.L., 2004. Timing and nature of the deepening of the Tasmanian Gateway. Paleoceanography 19, 4.

Stover, L.E., Partridge, A.D., 1973. Tertiary and late cretaceous spores and pollen from the Gippsland Basin, southeastern Australia. Proc. Royal Soc. Victoria 85, 237–286.

Tickell, S.J., Edwards, J., Abele, C., 1992. Port Campbell Embayment 1:100,000 Map Geological Report, Geological Survey of Victoria Reports. Geological Survey of Victoria, Melbourne.

van der Zwaan, G.J., Jorissen, F.J., Stigter, H.C., 1990. The depth dependency of planktonic/benthic foraminiferal ratios: constraints and applications. Mar. Geol. 95, 1–16.

van der Zwaan, G.J., Duijnstee, I.A.P., den Dulk, M., Ernst, S.R., Jannink, N.T., Kouwenhoven, T.J., 1999. Benthic foraminifers: proxies or problems? A review of paleoecological concepts. Earth Sci. Rev. 46, 213–236.

Vandenberghe, N., Brinkhuis, H., Steurbaut, E., 2003. The Eocene/Oligocene boundary in the North Sea area: A sequence stratigraphic approach. In: Prothero, D.R., Ivany, L.C., Nesbitt, E., Nesbitt, E.R., Nesbitt, E.A. (Eds.), From greenhouse to icehouse: the marine Eocene-Oligocene transition. Columbia University Press, pp. 418–436.

Wade, B.S., Pälike, H., 2004. Oligocene climate dynamics. Paleoceanography 19 (4).

Wade, B.S., Pearson, P.N., 2008. Planktonic foraminiferal turnover, diversity fluctuations and geochemical signals across the Eocene/Oligocene boundary in Tanzania. Mar. Micropaleontol. 68, 244–255.

Wade, B.S., Houben, A.J.P., Quaijtaal, W., Schouten, S., Rosenthal, Y., Miller, K.G., Katz, M.E., Wright, J.D., Brinkhuis, H., 2012. Multiproxy record of abrupt sea surface cooling across the Eocene-Oligocene transition in the Gulf of Mexico. Geology 40, 159–162.

Wade, B.S., Olsson, R.K., Pearson, P.N., Huber, B.T., Berggren, W.A., 2018. Atlas of Oligocene Planktonic Foraminifera. 46. Cushman Foundation for Foraminiferal Research Special Publication, pp. 1–528.

Waghorn, D.B., 1989. Middle Tertiary calcareous nannofossils from Aire District, Victoria; a comparison with equivalent assemblages in South Australia and New Zealand. Mar. Micropaleontol. 14, 238–255.

Wallace, M.W., Holdgate, G.R., Daniels, J., Gallagher, S.J., Smith, A., 2002. Sonic velocity, submarine canyons, and burial diagenesis in Oligocene-Holocene cool-water carbonates, Gippsland Basin Southeast Australia. AAPG Bull. 86, 1593–1607.

Zachos, J., Quinn, T.M., Salamy, K.A., 1996. High-resolution (104 years) deep-sea foraminiferal stable isotope records of the Eocene-Oligocene climate transition. Paleoceanography 11, 251–266.

Zachos, J., Pagani, M., Sloan, L., Thomas, E., Billups, K., 2001. Trends, Rhythms, and Aberrations in Global climate 65 Ma to present. Science 292, 686–693.

Zachos, J., Dickens, G.R., Zeebe, R.E., 2008. An early Cenozoic perspective on greenhouse warming and carbon-cycle dynamics. Nature 451, 279–283.

Zheng, Y.G., Pagani, M., Liu, Z.H., Bohaty, S.M., DeConto, R., 2013. A 40-million-year history of atmospheric CO2. Philos. Transac. Royal Soc. a-Math. Phy. Eng. Sci. 371.

Author/s:
Gallagher, SJ; Wade, B; Li, Q; Holdgate, GR; Bown, P; Korasidis, VA; Scher, H; Houben, AJP; McGowran, B; Allan, T

Title:
Eocene to Oligocene high paleolatitude neritic record of Oi-1 glaciation in the Otway Basin southeast Australia

Date:
2020-08-01

Citation:
Gallagher, S. J., Wade, B., Li, Q., Holdgate, G. R., Bown, P., Korasidis, V. A., Scher, H., Houben, A. J. P., McGowran, B. & Allan, T. (2020). Eocene to Oligocene high paleolatitude neritic record of Oi-1 glaciation in the Otway Basin southeast Australia. GLOBAL AND PLANETARY CHANGE, 191, https://doi.org/10.1016/j.gloplacha.2020.103218.

Persistent Link:
http://hdl.handle.net/11343/239072

File Description:
Published version